Effect of Al_2O_3/CuO Hybrid Nanoparticles Dispersion on Melting Process of PCM in a Triplex Tube Heat Storage

Ibrahim E. Sadiq
Assistant lecturer
University of Technology
Mechanical Engineering Department
Baghdad
Iraq

Sattar Aljabai
Professor
University of Technology
Mechanical Engineering Department
Baghdad
Iraq

Abdulhassan A. Karamallah
Professor
University of Al Salam
Mechanical Engineering Department
Baghdad
Iraq

This research conducts an experimental and theoretical investigation of the melting characteristics of a phase change material in a triplex tube heat storage. A three-dimensional model is simulated numerically employing Ansys Fluent software. The enthalpy porosity method is chosen for solving the phase transition of paraffin wax. A blend of equal-volume CuO and Al_2O_3 hybrid nano-additives was used as conductive material to enhance heat transfer in PCM, which can be considered the originality of this study. At first, the differential scanning calorimeter (DSC) analysis was performed to determine the paraffin thermo-physical properties. Various volume concentrations of 0.4%, 0.8%, 1.6%, and 3.2% were dispersed in paraffin. Besides that, the experiment was performed under different mass flow and inlet fluid temperatures to study the effect of these two parameters on the phase transition rate. The outcomes indicate that adding an Al_2O_3/CuO hybrid nanoparticle of volume fraction of 0.4-3.2% causes a reduction in total charging time between 10% and 19%. The result also showed that the theoretical efficiency boosts from 61.7% to 84.8% as heat transfer fluid (HTF) inlet temperature increases from 62 °C to 78 °C.

Keywords: Melting, Triplex-tube heat storage, Hybrid nano-PCM, Heat transfer enhancement

1. INTRODUCTION

Nowadays, there is a rapid rise in air pollution due to increased demand for fossil fuels around the world. Moreover, the price of fossil fuels is rising dramatically. Therefore, utilizing renewable energy to heat greenhouses can be an environmentally beneficial alternative to satisfy the demand for low-cost energy [1,2]. Most solar power units need storage devices to store the excess thermal energy between heat supply and demand. The stored energy can be utilized later. There are three main approaches to holding heat in thermal storage systems: (a) sensible heat, based on changing material temperature when it absorbs or rejects heat; (b) latent heat, according to phase change from solid to liquid and vice versa. (c) thermochemical, occurred through exothermal/ endothermal reaction [3,4]. Latent heat thermal storage units that contain phase change materials (PCMs) offer several favorable characteristics compared to other storage materials, including high volumetric thermal storage capacity [5], chemical stability, non-corrosiveness, and minor temperature change during melting and solidification process due to phase-transition phenomena [6,7].

Diverse phase change materials (PCMs) with various melting and freezing temperatures are used in these systems, including eutectic, organic, and inorganic materials [8,9]. Organic PCMs, for instance, paraffin and fatty acids, possess self-nucleating properties but lower thermal conductivity and higher cost [10]. These kinds of PCMs have been successfully implemented in many commercial and domestic applications, for exam–ple, solar air/water heating, refrigeration units, and spa–ce heating in buildings [11,12]. The inorganic PCMs, including salt hydrates, are distinguished by their relatively low cost and acceptable availability. How–ever, these materials have some issues related to phase segregation and incongruent melting. The eutectic PCMs consist of either organic substances or inorganic substances, or a blend of them [13]. Moreover, a eu–tectic PCM is a salt solution dissolved in water with a phase transition temperature of less than 0 °C. In addition to cost, selecting the suitable type of PCM in a specific application should fulfill the following ope–ration requirements: (i) a melting point should fall wit–hin the specified working temperature range of a given application, (ii) thermo-physical properties should be stable after many operation cycles, and (iii) high rate of nucleation is desired to prevent super-cooling and the intense crystal growth rate to satisfy the demands of thermal energy retrieve from the storage device. (iii) non-explosive, non-flammable, non-poisonous [14]. In general, the melting point scope of 0 □−65 □ is app–ropriate for domestic hot water systems [15]. The main problem of PCM is its low thermal conductivity, which makes the system take a longer time to complete melting and solidification. To solve this issue, diverse enhancement ways have been developed by authors. Some of these ways employ fins [16,17], metal mat–rices [18,19], heat pipes [20,21], and a more recent technique is to disperse high conductive nanoparticles in a PCM [22,23].

Received: August 2023, Accepted: October 2023
Correspondence to: Ibrahim E. Sadiq
Mechanical Engineering Department, University of Technology, Baghdad, Iraq
E-mail: me.19.27@grad.uotechnology.edu.iq
doi: 10.5937/fme2304606S
© Faculty of Mechanical Engineering, Belgrade. Allrights reserved

The utilization of shell and tube heat storage in conjunction with extended surfaces is favorable in various applications owing to its advantages in terms of heat transfer efficiency, manufacture simplicity, and easy implementation to systems. Mosaffa et al. [24] conducted a two-dimensional analytical study to examine the PCM solidification rate in a vertical double-pipe heat exchanger embedded with a radial fin. Their result showed that PCM placed in the cylindrical shell solidified faster than placed in the rectangular shell. Rathod and Banerjee [25] performed an experimental study of the phase transition process of stearic acid in a vertical shell and tube with three longitudinal fins. It was concluded that melting and solidification rates of stearic acid enhanced by 24.52% and 43.6%, respectively. This was attributed to the fact that installing fins increases heat diffusion in PCM. Later, Rabienataj Darzi et al. [26] reported that the phase change rate of n-eicosane was affected by a number of longitudinally extended surfaces in shell and tube. According to the numerical analysis, the duration for both melting and solidification processes decreased by 39–82% and 28–85% by increasing the number of fins from 4 to 20 compared to storage without fins. Furthermore, Lohrasbi et al. [27] observed that attaching longitudinal, circular, and v-shaped fins to the outer tube surface of vertical shell and tube augments the melting rates of PCM by 3.26, 3.55, and 4.28 times in comparison to storage without fin. Safari et al. [28] analyzed experimentally and numerically the charging rate in concentric and eccentric heat storage. Results revealed that eccentric heat storage equipped with tree-shaped fins reduces the charging period by 85%. The same authors in the study [29] proposed a novel non–uniform arrangement of tree-shaped fins. Results indicated that all the tree-shaped fins attached in the lower PCM reduce the melting time by 9.25% in comparison to the uniform distribution of tree-shaped fins. Wang et al. [30] experimentally investigated the melting rate of paraffin-embedded with aluminum foam. According to their findings, the incorporation of aluminum foam into PCM was able to augment the rate of charging and improve the temperature homogeneity of PCM. Compared to pure paraffin, PCM's total melting duration with aluminum foam decreased by 26.4% and 25.6% when the heat fluxes boosted from 7000 W/m^2 to 12000 W/m^2, respectively. Li et al. [31] examined the heat transfer characteristic of paraffin with copper foam. The outcome showed that the enhancing thermal conduction was more significant than the diminishing convection current during melting.

As we noticed from the abovementioned review, extended surfaces, and metal foam have good potential to enhance heat transfer. However, they have undesirable consequences: (i) reducing heat storage due to decreased PCM volume and (ii) boosting the weight of the thermal storage system. Therefore, the addition of nanoparticles is an alternative technique to enhance the effective thermal conductivity with relatively little increase in overall weight. Nanoparticles can be categorized into two groups: (a) carbon allotropes and (b) metal-oxides or metals [32], carbides, and nitrides [33].

Enhancing the performance of PCM using nano-scale powder was first investigated by Khodadadi and Hosseinizadeh [34]. In the research, water was used as PCM dispersed with copper nanoparticles. Results showed that adding nanoparticle speed up the heat transfer rate during solidification. This is encouraging for best usage in heat storage applications. Wu et al. [35] presented an experimental study on the charging and discharging of paraffin as a PCM incorporated with nanoparticles. It was reported that paraffin with 2% by weight copper nanoparticle can increase thermal conductivity by 14.2% and 18.1% in solid and liquid phases, respectively. The incorporation of graphene, carbon nano-tubes, Al, and TiO2 nano-powder in paraffin was experimentally studied by Warzoha and Fleischer [36]. The outcome revealed that the overall durations of melting and solidification for paraffin mixtures were respectively shortened by 29.82%, 27.19%, 16.67%, and 12.22%. Furthermore, the quantity of accumulative heat was enhanced by 11% for the graphene/PCM mixture. However, decreases ranging between 15–17% were observed for other nanoparticles. Hamza and Aljabair [37] stated that the inclusion of two different types of nanoparticles has a high potential to augment heat transfer due to their synergistic impact. Alizadeh et al. [38] outlined through numerical simulations that shape factors of nano-additives affect the discharging rate for PCM with TiO2–Cu hybrid nano-additives. It was observed that because of the comparatively higher shape factor, the heat release rate for lamina nanoparticles was higher than for hexahedrons and platelets.

In contrast, the overall accumulative heat was decreased with an increased shape factor. Hosseinzadeh et al. [39] stated that the heat release rates for Al_2O_3–Go hybrid nano-additives with 2.5% and 5% by volume were 1.74 and 2.69 times higher than the case without nano-additives. In the same way, as performed in [40], shell and tube were employed to store paraffin wax integrated with Al_2O_3, AlN, and graphene nanoparticles. It was observed that a volume fraction of 1% of nano-additives can improve the melting rate by 28.01%, 36.47%, and 44.57%, and the solidification rate by 14.63%, 34.95%, and 41.46%, respectively. Said and Hassan [41] modified the conventional condenser of an air-conditioning system with a heat exchanger containing nano-enhanced PCM. It was exhibited that the inclusion of 5% by volume of Al2O3, CuO, and Cu nanoparticles into PCM can enhance the power saving up to 7.28%, 7.35%, and 7.41%, respectively, as compared to 7.18% power saving for pure PCM case. Various types of studies are discussed, with information regarding the method of study and type of process displayed in Table 1. It is obvious that employing nanoparticles speeds up the melting and solidification process. Kumar et al. [42] performed an experimental study to discover the thermal efficiency of a refrigerator by implementing the PCM and nano-PCM on the condenser side. Paraffin wax and a mixture of paraffin wax /Multi-Walled Carbon Nano Tube were used as storage media on the condenser side. It was observed that the utilization of PCM and nano-PCM can

respectively result in energy savings of about 13.06% and 18% for refrigerators.

Implementing heat storage-based PCM is crucial for optimal utilization of solar energy. Solar thermal units, for example, solar parabolic-trough collectors, can be used for a variety of purposes, including desalination, air heating units for food drying processes and buil–dings, refrigeration units, electrical power generation, and industrial applications [43]. The utilization of flat plate solar collectors for the purpose of drying proces–ses has also been reported by Fudholi and Sopian [44].

TTHS with nano-PCM can be applied for heat recovery applications. Waste heat that is produced from industry or domestic heating units can be utilized to heat up water for industrial or household use, resulting in energy savings and a reduction in greenhouse gas emissions. In a recent study conducted by Cao et al. [45], they implemented a TTHS device to extract energy from a direct evaporative ammonia refrigeration unit. Carnauba wax/expanded graphite as PCM is inserted into the intermediate tube of TTHS with refrigerant and water passing through the inner tube and outer annulus, respectively. The PCM existed in the intermediate tube, absorbing thermal energy from the refrigerant and subsequently releasing this energy to the water.

Nascimento Porto et al. [46] have suggested using a TTHS with paraffin to operate a liquid-desiccant air conditioning unit. The authors used a solar panel to heat up HTF, which passes through the inner tube and outer annulus of TTHS. Afterward, the heat will be trans–ferred to the RT82 (PCM) located within the inter–mediate tube of TTHS. Likewise, Al-Abidi et al. [47] utilized a solar collector with evacuated tubes to provide HTF with solar energy. The arrangement of HTF and paraffin is identical to the numerical work performed by Nascimento Porto et al. [46].

In this paper, n experimental and numerical inves–tigation is conducted to examine the melting process of PCM dispersed with Al_2O_3-CuO hybrid nanoparticles in a triplex tube heat storage (TTHS). Paraffin wax, as the PCM, is placed in an annulus gap between the intermediate tube and the inner tube while the water flows in the inner tube and outer shell. TTHS has a larger heat transfer area and, thus, a higher charging rate than double-pipe heat storage. The literature revealed that there needs to be more studies regarding the phase transition characteristic of hybrid-nano PCM in TTHS. Therefore, the novelty of this work is to determine the effect of hybrid nanoparticle inclusion on heat transfer behavior during PCM melting in TTHS. The other target of this article is to study the effect of the operation parameters (HTF inlet temperature and mass flow rate) on the charging process. The major steps of the current work are outlined in the figure 1.

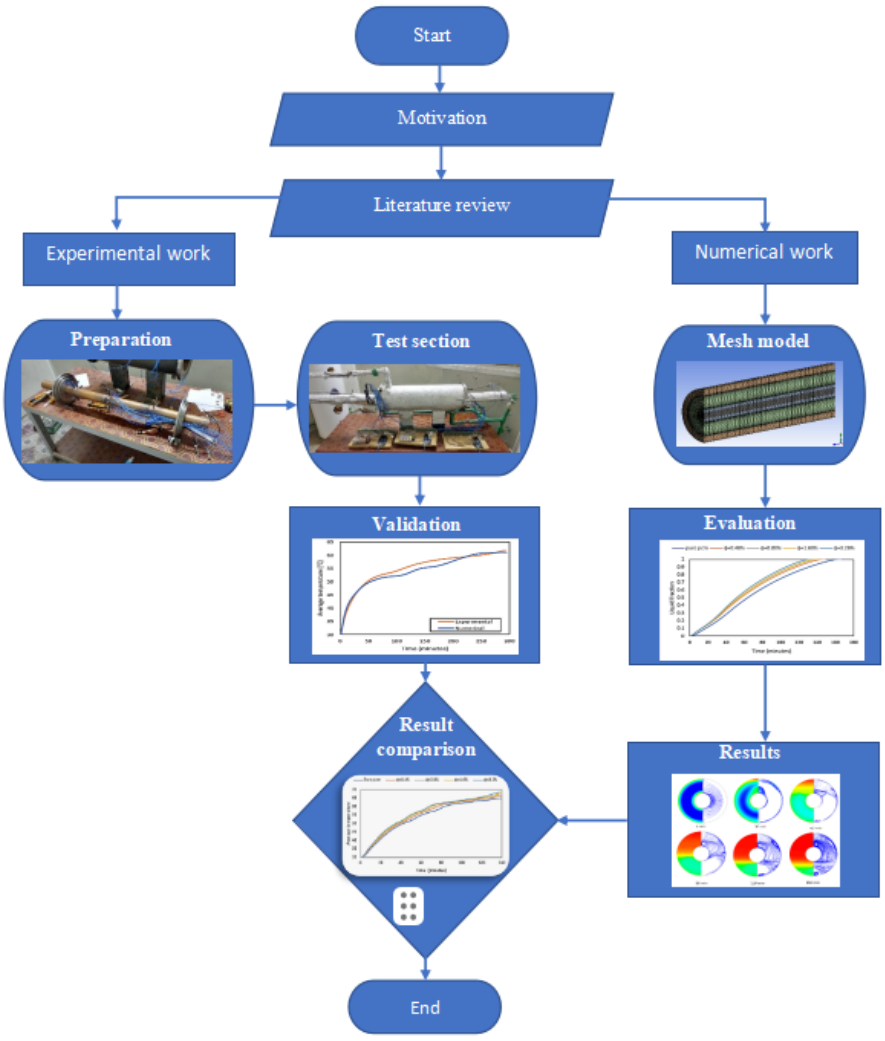

Figure 1. The major steps of current work.

Table 1. Summary of studies on nano-enhanced PCM.

Ref.	method	process	PCM	Nano-type	Main result
[34]	Num.	Discharging	water	Cu	Solidification rate increases with increased volume fraction of nanoparticle.
[35]	Exp.	Charging and discharging	paraffin	Cu	Increase thermal conductivity up to 18.1% in the solid phase by adding 2 wt % Cu.
[36]	Exp.	Charging and discharging	paraffin	Al and TiO2 nano-powder	Maximum solidification time reduction was 29.82% by adding graphene nanoparticles.
[38]	Num.	Discharging	water	TiO2–Cu hybrid nano	The shape factors of nano-additives significantly affect discharge rate and thermal energy storage.
[39]	Num.	Discharging	water	Al2O3–Go hybrid nano	Heat release rate is 2.69 times higher than the case without nano-additives.
[40]	Exp. And Num.	Charging and discharging	paraffin wax	Al_2O_3, AlN, and graphene nano	The highest improvement in melting and solidification rates was 44.5% and 41.4%, respectively.
[41]	Exp. And Num.	Charging and discharging	paraffin wax	Al2O3, CuO and Cu nano	Dispersion of 5% by volume Cu nanoparticle can save the air conditioning system's power by 7.41%.
Present work	Exp. And Num.	Charging	paraffin wax	Al2O3, CuO hybrid nano	An 18.6% reduction in melting duration was achieved by adding 3.2% hybrid nanoparticles.

2. EXPERIMENTAL EQUIPMENT AND TEST PROCEDURE

2.1 Experimental setup

The energy storage system is a triplex tube heat storage oriented horizontally with 7 kg of PCM placed between inner and intermediate tubes. Figure 2 and Figure 3 demonstrate the schematic sketch and photo of the test rig employed for this study. As can be seen, there are two cycles of water: the hot water cycle, in which heat is transferred from hot water to PCM, and the cold-water cycle, in which stored energy in PCM is transferred back into cold water. Figure 4 illustrates the sectional view of the test section, which consists of three horizontally oriented concentric tubes 600 mm long. The radius of inner tube (Ri), intermediate tube (Rint) and outer tube (Ro) are 25 mm, 150 mm, and 200 mm, respectively. Both inner and intermediate tubes are made of copper to minimize thermal resistance. However, the outer tube is made of carbon steel. To seal both ends of the heat storage, two circular carbon steel flanges with a 53 mm diameter central hole to enable the passage of the inner tube were provided on both ends. Each flange has a small hole of 10 mm diameter to allow passage of thermocouple wires. Glass wool thermal insulator of 50 mm thickness, and 0.04 w/mk thermal conductivity is wrapped around the heat storage to minimize heat dissipation.

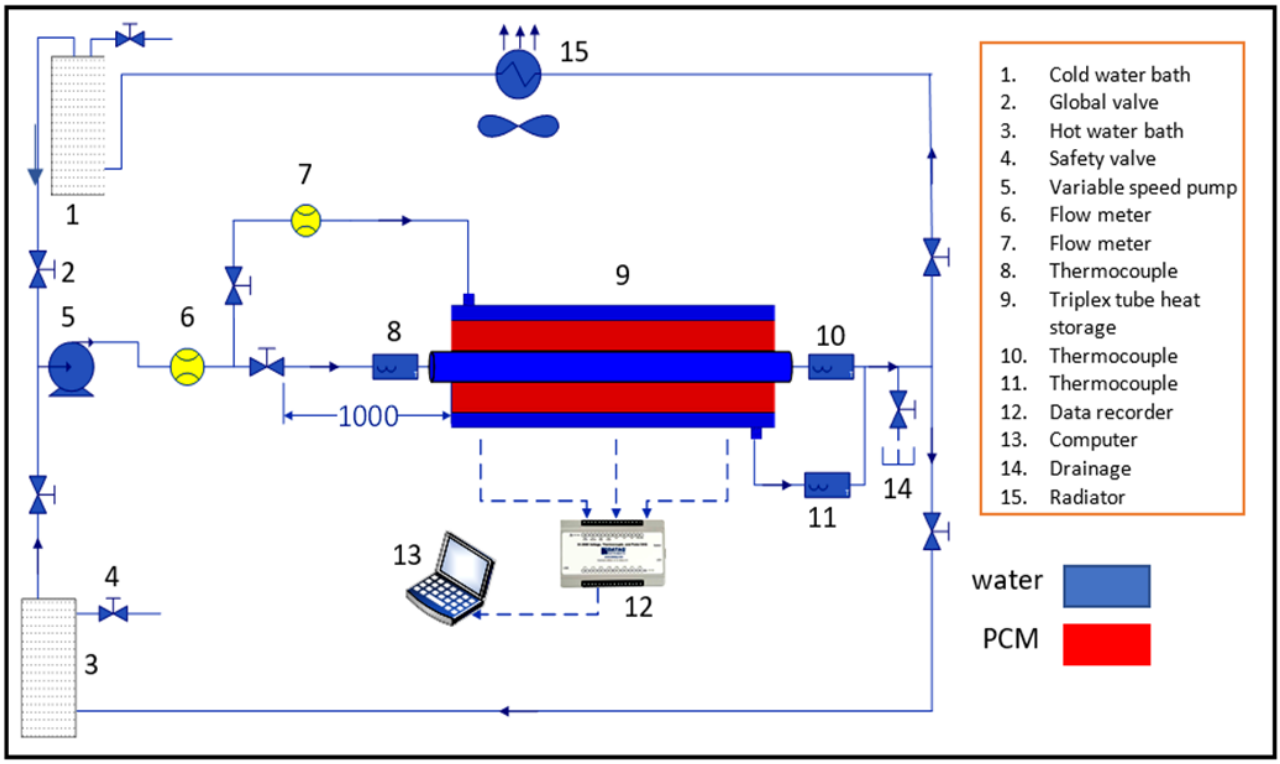

Figure 2. Schematic sketch of test rig.

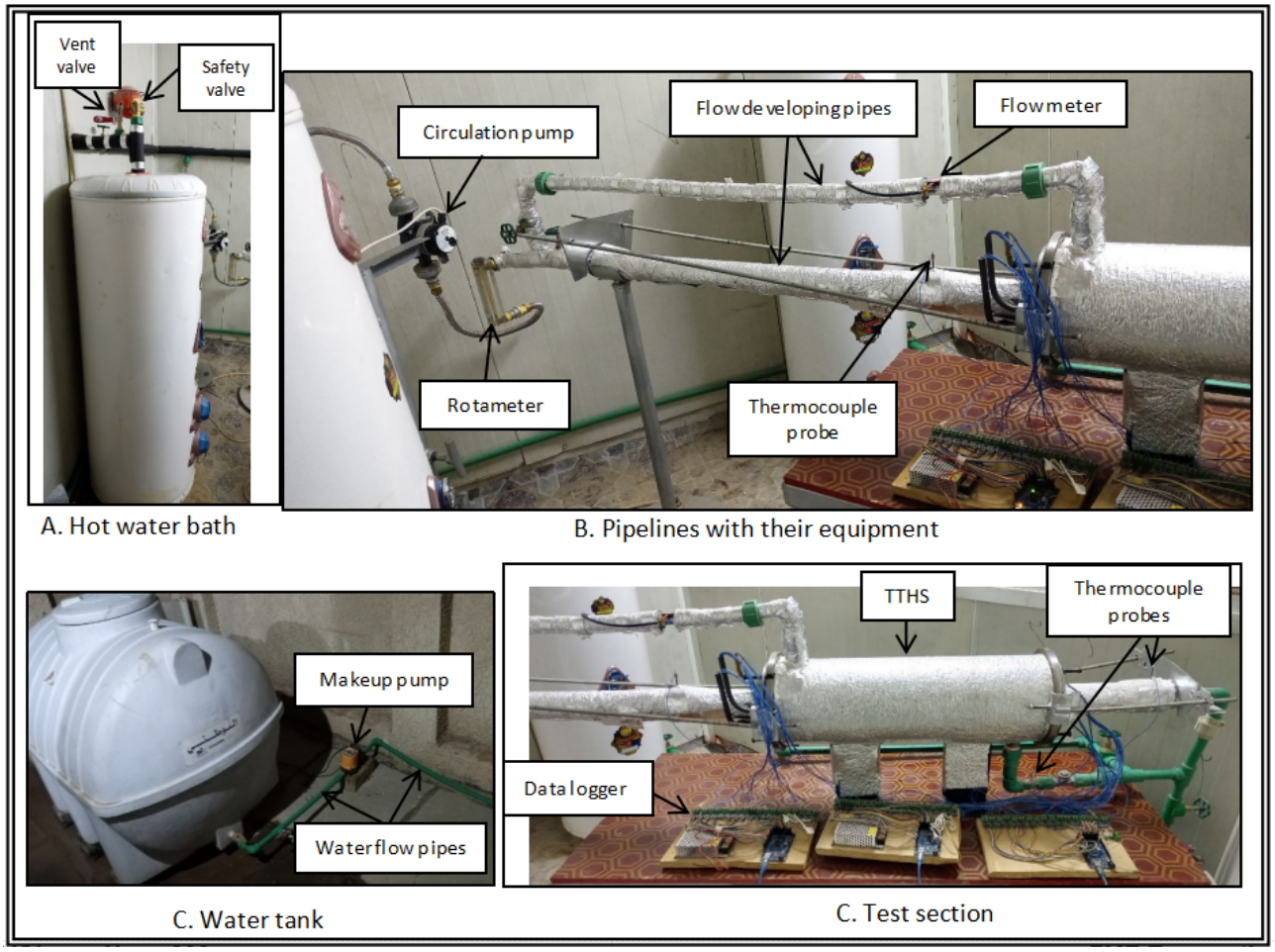

Figure 3. Photo of test rig parts

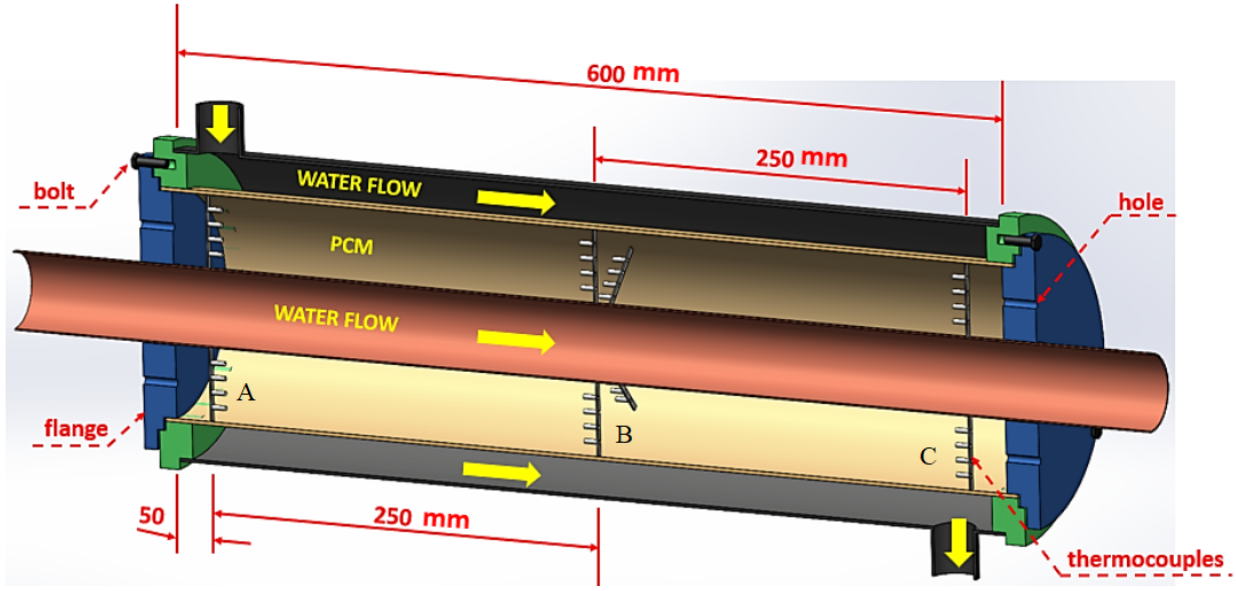

Figure 4. Sectional sketch of the triplex tube heat storage

To measure the temperature distribution of PCM, sixty K-type thermocouples were fixed in PCM and distributed equally in three sections along the axial direction. Namely, sections A, B, and C, see figure 4. Each section has 20 thermocouples distributed in radial and angular directions, as depicted in Figure 5. Besides that, one thermocouple fitted in the inlet to measure the water inlet temperature and two thermocouples in the outlet to measure the outlet water temperature. One on the tube side and the other on the shell side. All the thermocouples with a temperature recording range of 0–200 °C and a precision of ±0.3 °C were linked to a data logger, which connected to a computer. Furthermore, a rotameter with 4% accuracy was used to measure the flow rate of HTF.

Water tanks of 250 liters equipped with a 1500-watt electrical heating coil and thermostat were used to increase water temperature and maintain it at a constant

value. At the beginning of the experiment, turn on the water heater to heat up the water temperature to a pre-determined value. After reaching the required tem–perature, the main circulation pump was run to supply hot water to heat storage, where hot water releases its heat into PCM, and the melting process started. The low flow temperature attained from the outlet of heat storage is returned to the tank to redo the cycle.

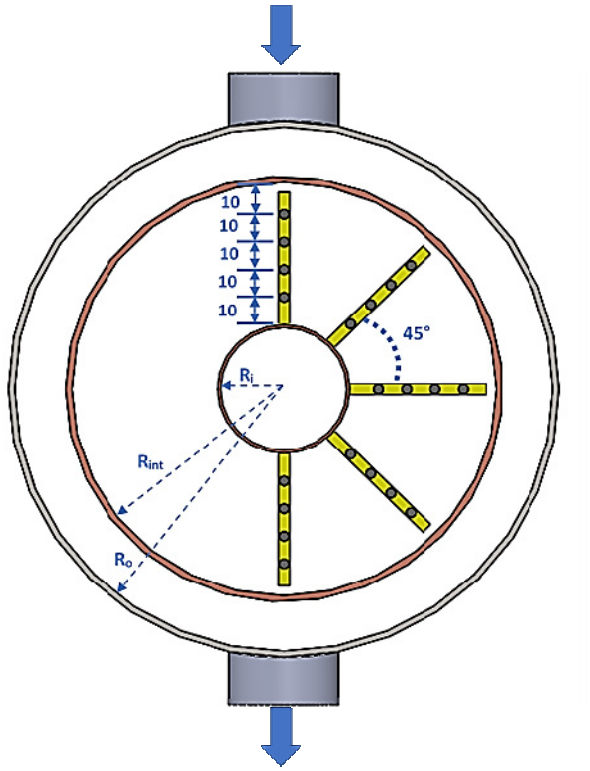

Figure 5. Schematic sketch of thermocouple distribution.

2.2 PCM selection

According to previous works, organic PCMs have a high heat of fusion per unit mass, are chemically inert, non-corrosiveness, and are more stable during the charging cycle compared to hydrated salts and non-paraffin organics. It is very appropriate for the SAHP heating system application. Therefore, paraffin of 53 °C melting temperature was chosen. This temperature was chosen because the Iraq weather is sunny and solar radiation is high most of the year; the PCM can absorb the highest possible heat from the solar collector, especially throughout the summertime. Differential Scanning Calorimeter (DSC) was used to examine the fusion's transition temperature and latent heat. 14.6-gram sample of paraffin was heated between 40 °C and 900 °C with heating rates of 20 °C/min as demonstrated in figure 6. The phase transition temperature range can be calculated between the onset temperature and temperature matching the peak of the curve. In contrast, the latent heat of fusion is determined by integrating the area under the peak of the curve. The result obtained from this test is written in Table 2.

2.3 Hybrid nano PCM preparation

Hybrid nano-additives were achieved by thoroughly mixing equal volume Al_2O_3 and CuO nanoparticles in a clean vessel. Then, different hybrid nano concentrations of 0.4%, 0.8%,1.6%, and 3.2% were dispersed in molten PCM. The selection of these volume fractions is based on the previous studies, as they stated that the low volume fraction of nanoparticles is preferable because high volume fraction causes particle agglomeration, latent heat reduction, and high material cost [48,49].

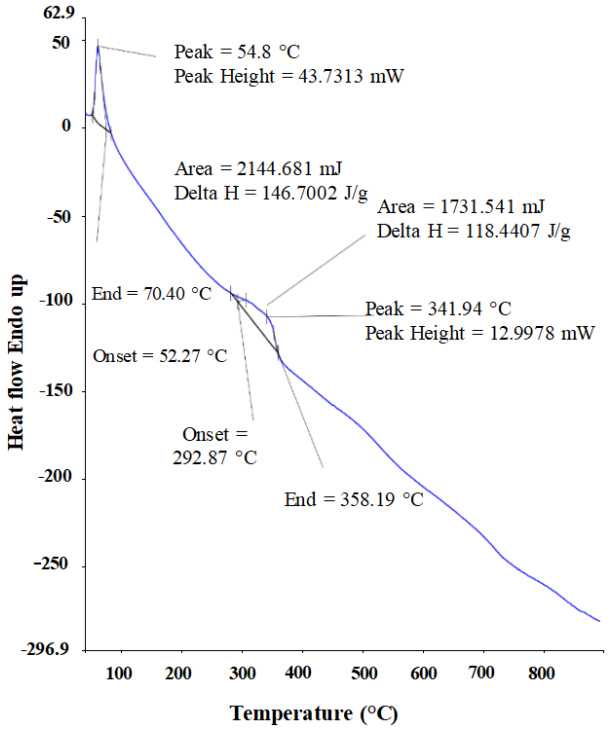

Figure 6: Heat transfer variation vs temperature for tested paraffin wax.

To prepare hybrid-Nano PCM, the first PCM is heated by using a hot water bath. Then, the hybrid nanoparticles of specific volume fraction were dispersed gradually to the molten PCM at a steady rate. Simultaneously heating and agitating the compound on the mechanical stirrer for 30 minutes to attain a homogeneous mixture. Finally, the prepared mixture was added gradually (layer after layer) into the annulus to prevent the creation of air voids in the paraffin. An adequate amount of time was provided to solidify every liquid layer, and then the subsequent liquid layer was poured into storage. Similar steps were repeated until the entire annulus was filled with PCM. The whole preparation steps are detailed and visualized in Figure 7.

The total volume concentration of hybrid nano–particles in the mixture [50]:

$$\varphi_{hnpcm} = \varphi_{np1} + \varphi_{np2} \tag{1}$$

Density of hybrid nano-PCM [50,51]:

$$\rho_{hnpcm} = \varphi_{np1}\varphi_{np2} + \varphi_{np2}\rho_{np2} + \left(1-\varphi_{np1}-\varphi_{np2}\right)\rho_{pcm} \tag{2}$$

Specific heat of hybrid nano-PCM [50,51]:

$$C_{p,hnpcm} = \frac{\left(\varphi_{np1}C_{p,np1}\rho_{np1} + \varphi_{np2}C_{p,np2}\rho_{np2} + \left(1-\varphi_{np1}-\varphi_{np2}\right)C_{p,pcm}\rho_{pcm}\right)}{\rho_{hnpcm}} \tag{3}$$

The viscosity of hybrid nano-PCM base on the Batchelor model [52]:

$$\mu_{hncpm} = \left(1 + 2.5\varphi_{hnpcm} + 6.2\left(\varphi_{hnpcm}\right)^2\right)\mu_{pcm} \quad (4)$$

The thermal conductivity of hybrid nano-PCM is predicted according to the Maxwell model [53]:

$$\frac{k_{hnpcm}}{k_{pcm}} = \left(\frac{k_{hnp} + 2k_{pcm} + 2\left(\varphi_{np1}k_{np1} + \varphi_{np2}k_{np2}\right) - 2\varphi_{hnpcm}k_{pcm}}{k_{hnp} + 2k_{pcm} - 2\left(\varphi_{np1}k_{np1} + \varphi_{np2}k_{np2}\right) + 2\varphi_{hnpcm}k_{pcm}}\right) \quad (5)$$

where (k_{hnp}) is an equivalent thermal conductivity of hybrid nanoparticles, which can be estimated as follows [50]:

$$k_{hnp} = \frac{\left(\varphi_{np1}k_{np1} + \varphi_{np2}k_{np2}\right)}{\varphi_{hnp}} \quad (6)$$

Latent heat of fusion of hybrid nano-PCM [54,55]:

$$L_{hnpcm} = \frac{\rho_{pcm}\left(1 - \varphi_{np1} - \varphi_{np2}\right)}{\rho_{hnPCM}} \quad (7)$$

The thermophysical properties of CuO and Al_2O_3 nano-powder and hybrid nano-PCM's thermal characteristics are listed in Tables 2 and 3.

Table 2. Thermophysical properties of paraffin and nanoparticles [56,57].

Properties	Pure PCM	Al_2O_3	CuO
Density (kg/m3)	$\frac{750}{0.001(T-319.15)+1}$	3970 [58]	6500 [56]
Specific heat (J/kg °C)	2149	765 [56]	535.6 [56]
Thermal conductivity (w/m °C)	0.21 if $T < T_{solidus}$ 0.12 if $T > T_{liquidus}$	36 [57]	18 [57]
Viscosity (pa.s)	$0.001\exp\left(-4.25 + \frac{1790}{T}\right)$	-	-
Latent heat of fusion (J/kg)	146700	-	-
Solidus tempe–rature, °C	52	-	-
Liquidus tem–perature, °C	54	-	-

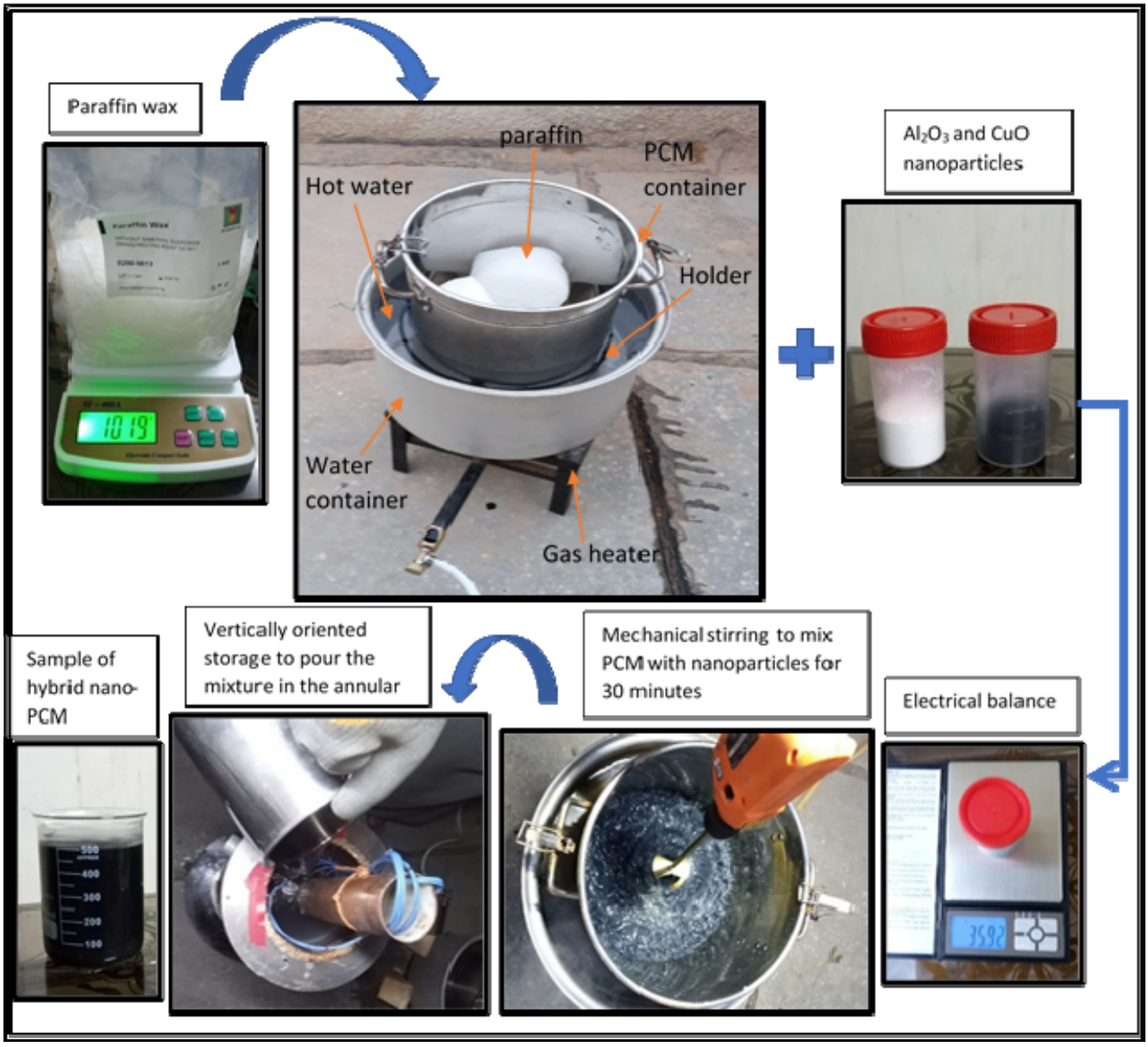

Figure 7. Hybrid nano-PCM preparation procedure.

Table 3. Thermophysical properties of hybrid nano-PCM.

Properties	0.4%	0.8%	1.6%	3.2%
Density (kg/m3)	762.5	780.3	815.8	886.8
Specific heat (J/kg °C)	2107.5	2068	1994	1864
Thermal conductivity (S) (w/m °C)	0.2133	0.21668	0.2235	0.2381
Thermal conductivity (L) (w/m °C)	0.1219	0.12385	0.1278	0.13619
Viscosity (pa.s)	0.00362	0.00381	0.0042	0.0056
Latent heat of fusion (J/kg)	142710	138901	131782	119255

2.4 Nanostructure of nanoparticles and composites

The powder X-ray diffraction (XRD) analysis was conducted using a Bruker AXS D8 Advance X-ray diffractometer, employing Cu-Kα radiation within the range of 5–60°. The diffraction peaks at 2θ = 19.50° (013), 32.80° (022), 34.60° (117), 36.76° (122), 39.50° (026), and 45.64° (220) confirm the form of the Al2O3, see Figure 8. When the volume concentration of Al2O3 and CuO was maintained at 0.4 %, a lower quantity of nanoparticles was inserted in pure paraffin. Therefore, the physical alterations noticed in mono and hybrid nano-PCM were insignificant. XRD analysis indicated that both the mono and hybrid-nano-PCM have peaks of Al2O3 and CuO. By employing the Scherrer formula, the average particle size of the Al2O3, CuO, and their hybrid powder was estimated to be 17, 32, and 23 nm, respectively.

Figure 9 displays an inspection of the microstructure and surface morphology of mono-nano-PCM and their hybrid conducted using the ESEM. The uniform dispersion of nanoparticles in paraffin, as depicted in Figure 9, is attributed to the repulsive bonding of the inserting substance, as evidenced by the presence of white zones. Despite the fact that nanoparticle concenstration is constant and low, all nanoparticles are sufficiently mixed and implanted to reveal their existence in the mixture. Additionally, the homogeneous and heterogeneous migration of nanoparticles in paraffin can be visually distinguished through the analysis of LFD (Low-Field Diffusion) and BSED (Back-Scattered Elec–tron Diff–raction) pictures. Referring to Figure 9, the existence of regions defined by heterogeneous aggre–gation of nanoparticles and paraffin is vividly identified. Refe–rences [59] and [60] have documented a similar finding of nanoparticles migrating in a mixture. The micro–structure of the powder sample manifests that the par–ticles are in the form of tiny agglomerates and almost spherical in shape.

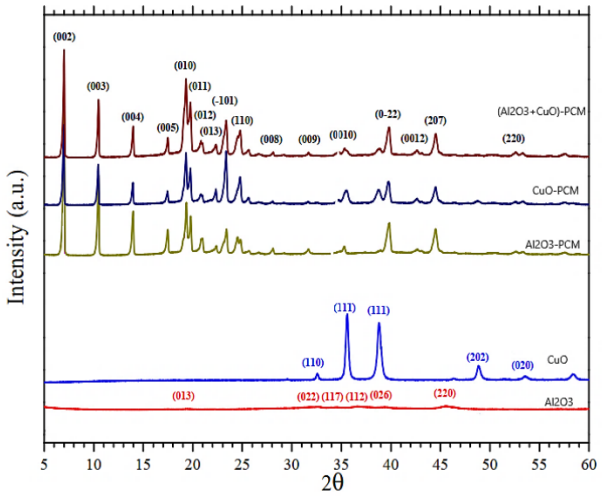

Figure 8. XRD data of Al2O3, CuO, and mono nano-PCM and hybrid nano-PCM.

2.5 Data reduction

The quantity of stored energy and storage efficiency can be theoretically calculated from the equations listed in Table 4.

Table 4. Energy equations and theoretical efficiency.

Variables	Equations
Heat transfer rate	$q_{total} = \left(\dot{m} c_{p,HTF} \left(T_{in} - T_{out}\right)\right)$
Accumulative energy [61]	$Q_{charging} = \sum_0^t q_{total} \Delta t$
Maximum heat storage	$Q_{\max} = M_{PCM}\left[C_{P,PCM}\left(T_{solidus} - T_{ini}\right) + (L) + C_{P,PCM}\left(T_{end} - T_{liquidus}\right)\right]$
Heat storage efficiency [62]	$n_{theory} = \dfrac{Q_{charging}}{Q_{\max}}$

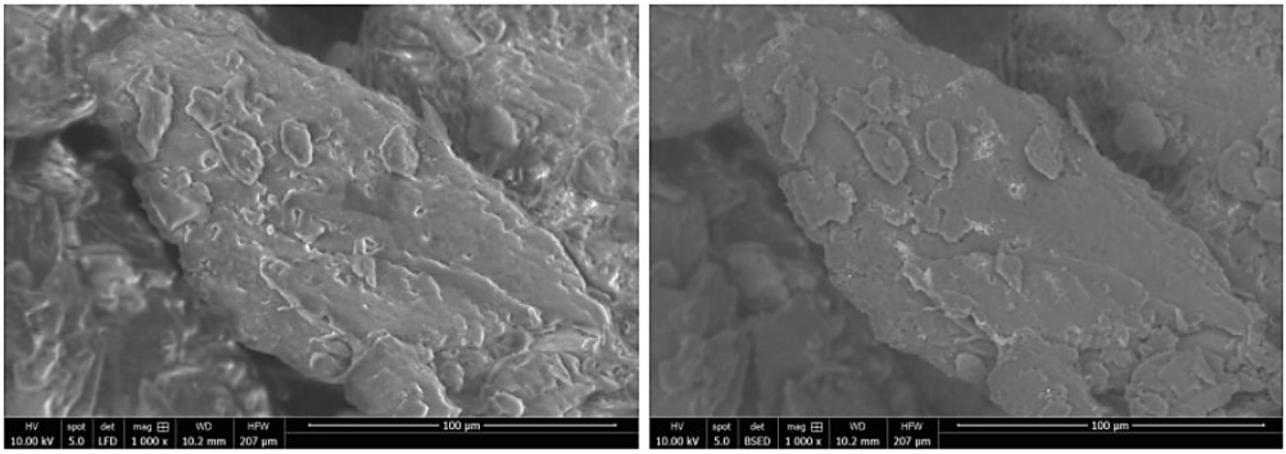

a) b)

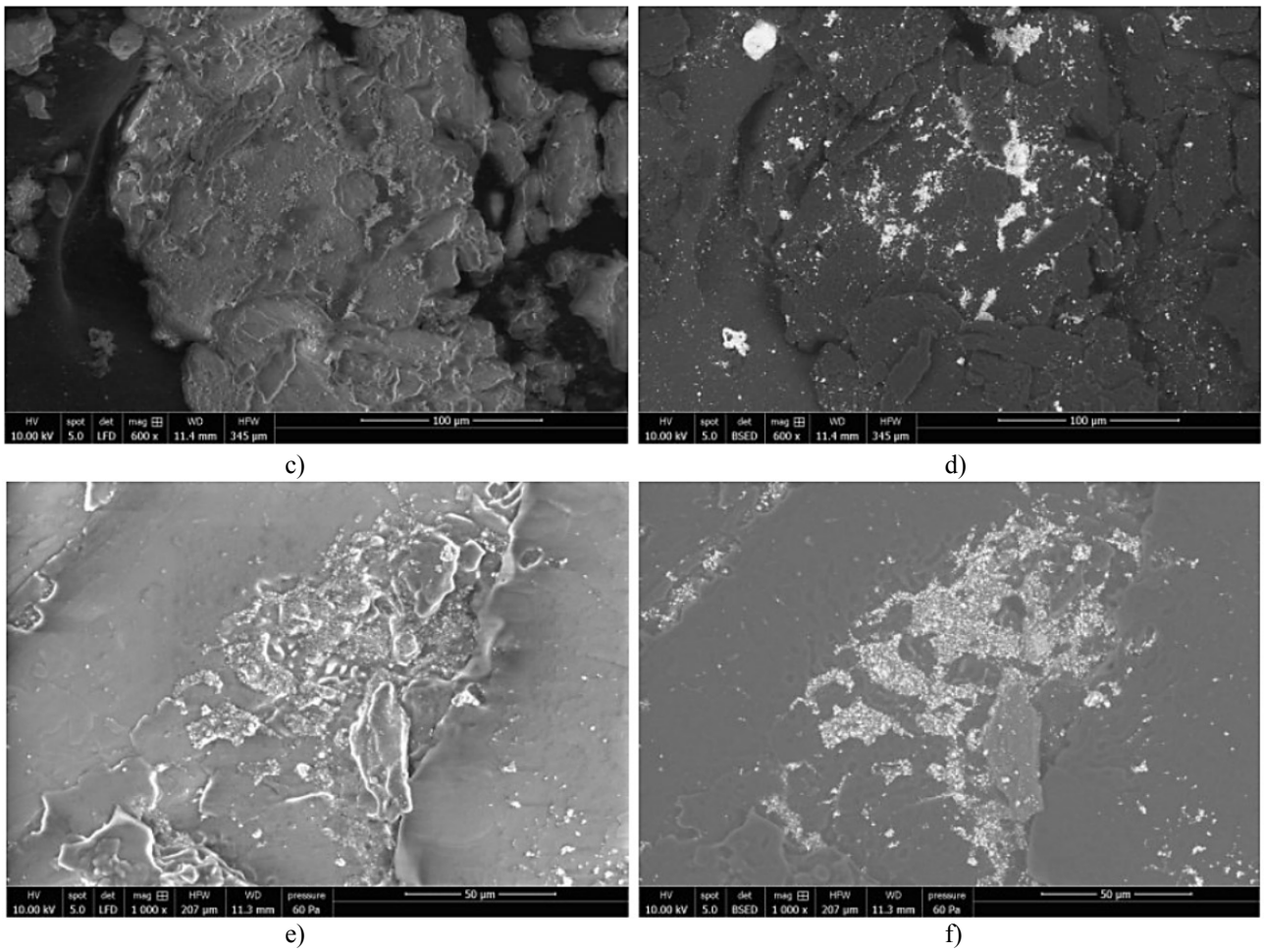

Figure 9. ESEM photo of Al2O3-PCM (a) LFD and (b) BSED, CuO-PCM (c) LFD and (d) BSED, and (Al2O3+CuO)-PCM (e) LFD and (f) BSED.

2.6 Uncertainty analysis

Because of measurement device errors, uncertainty analysis is required. The analysis was performed based on Robert J. Moffat [63]. The independent variables tested in the current study are the inlet, outlet tempe–rature, and mass flow rate. The total uncertainty of heat transfer for different mass flow rates is presented in Table 5.

Table 5. Uncertainty for hybrid nano-PCM (φ = 0.4%).

Mass flow rate (kg/min)	Uncertainty (w)	Relative uncertainty
3	7.896	0.02039
6	5.177	0.01077
9	4.194	0.00777
12	3.761	0.00640

(R) is estimated as follows:

$$\delta RX_i = \frac{\partial R}{\partial X_i} * \partial X_i \tag{1a}$$

$$S_R = \left[\sum_{i=1}^{m} \left(\frac{\partial R}{\partial X_i} * \partial X_i \right)^2 \right]^{-0.5} \tag{1b}$$

S_R is the uncertainty in the result, which can be expressed as:

$$S_R = \left[\left(\frac{\partial R}{\partial X_1} S_{X1} \right)^2 + \left(\frac{\partial R}{\partial X_2} S_{X2} \right)^2 + \ldots\ldots + \left(\frac{\partial R}{\partial X_i} S_{Xi} \right)^2 \right]^{-0.5} \tag{1c}$$

The heat transfer (Q) which is the function of two variables:

$$Q = f\left(\dot{m}, \Delta T\right) \tag{1d}$$

$$\frac{\partial Q}{\partial \dot{m}} = C_p \Delta T \tag{1e}$$

$$\Delta T = T_{in} - T_{out} \tag{1f}$$

$$\frac{\partial Q}{\partial \Delta T} = \dot{m} C_p \tag{1g}$$

The uncertainty of the heat transfer (S_Q) is given as follows:

$$S_Q = \left[\left(\frac{\partial Q}{\partial \dot{m}} S_{\dot{m}} \right)^2 + \left(\frac{\partial Q}{\partial \Delta T} S_{\Delta T} \right)^2 \right]^{1/2} \tag{1h}$$

$$Relative\,uncertainty = \frac{S_Q}{Q} \tag{1i}$$

3. NUMERICAL METHOD

3.1 Governing equations

The enthalpy porosity approach [64,65] is employed in this investigation to simulate the phase transition beha–vior of the nano-PCM. To facilitate the mathematical model, certain assumptions are made, as follows:

- The flow is considered transient, laminar, and three-dimensional.
- The term of viscous dissipation is neglected. Therefore, the temperature variation and viscous flow in the PCM are described by thermal energy and Navier–Stokes equations, respectively.
- Density, viscosity, and thermal conductivity are functions of temperature, while temperature-inde–pendent thermophysical properties of specific heat.
- Fully developed HTF in both tube and shell sides is assumed.
- Heat exchange between the storage and surroundings is negligible.

Continuity equation [66,67]:

$$\frac{\partial \rho}{\partial t} + \nabla \cdot \left(\rho \vec{V} \right) = 0 \tag{8}$$

Momentum equation:

$$\frac{\partial \vec{V}}{\partial t} + \vec{V} \cdot \nabla \vec{V} = \frac{1}{\rho} \left(-\nabla P + \mu \nabla^2 \vec{V} + \rho \beta \vec{g} \left(T - T_{ref} \right) \right) + \vec{S} \tag{9}$$

Thermal energy equation:

$$\frac{\partial h}{\partial t} + \frac{\partial H}{\partial t} + \nabla \cdot \left(\vec{V} h \right) = \nabla \cdot \left(\frac{k}{cp} \nabla h \right) \tag{10}$$

The enthalpy of the material is computed as the sum of the sensible enthalpy, h, and the latent heat, ΔH [68]:

$$H = h + \Delta H \tag{11}$$

where

$$h = h_{ref} + \int_{T_{ref}}^{T} C_p dT \tag{12}$$

The latent heat content is formulated in relation to the latent heat of the substance, denoted as:

$$\Delta H = \lambda L \tag{13}$$

ΔH can range from zero (solid) to L (liquid). Hence, the liquid fraction, denoted as λ, could be characterized as:

$$\lambda = \begin{cases} \dfrac{\Delta H}{L} = 0 \; if \; T < T_{solidus} \\ \dfrac{\Delta H}{L} = 1 \; if \; T > T_{liquidus} \\ \dfrac{\Delta H}{L} = \dfrac{T - T_{solidus}}{T_{liquidus} - T_{solidus}} if \; T_{solidus} < T < T_{liquidus} \end{cases} \tag{14}$$

Since phase transition effects on convective heat transfer, Darcy's law $\vec{S}$ (as source term) is added to the momentum equation in equation (9), which is defined as [69]:

$$\vec{S} = \frac{(1-\lambda)^2}{\lambda^3} A_{mush} \vec{V} \tag{15}$$

The coefficient A_{mush} is a mushy zone value. In most cases, this coefficient ranges between 10^4–10^7 [70]. In the present simulations, A_{mush} is considered a fixed value that is set to 10^6.

3.2 Initial and boundary conditions

The initial temperature of HTF and PCM are set to 30 °C, and PCM is in solid phase. Regarding the boundary condition, the type of “mass-flow-inlet” (of constant value and constant temperature) is selected for the HTF at the inlet of the tube and shell sides of storage. The inlet HTF mass flow rate is estimated from the inlet volumetric flow rate and density of water. The total flow rates of HTF range from 3 kg/min to 12 kg/min, while the temperatures of HTF vary from 62 °C to 78 °C. It is worth mentioning that the HTF inlet flow rate and inlet temperature remained constant during the charging. In addition to the inlet boundary condition, the outlet boundary condition of the HTF is chosen as "mass-flow-outlet.” Moreover, the boundary condition of outer surfaces is selected as adiabatic since well insulated the outer surface of storage. No-slip boundary condition on the tube surfaces was chosen.

3.3 Numerical procedure and verification

The simulation was done using Ansys FLUENT 2021 software based on the finite volume approach and the enthalpy–porosity method, as detailed by Patankar [71]. In this method, the calculation is determined by a fixed grid, and the governing equations were adapted to be valid for solid and liquid phases. The mushy zone is the zone where the liquid and solid phases exist together. This region is exhibited as a "pseudo" porous medium where porosity increases from 0 (solid) to 1 (liquid) as the material melts. More information regarding the application of computational fluid dynamics in latent heat energy storage is detailed in the paper [72].

The SIMPLE algorithm [71] within a 3D in-house developed code [73] is adopted for solving pressure-velocity coupled equations. The PRESTO scheme is implemented for the pressure correction equation, whe–reas the second-order upwind scheme is applied for resolving the energy and momentum equations. The values of under relaxation factors for liquid fraction, momentum, pressure, and energy are 0.9, 0.6, 0.3, and 1, respectively. To obtain accurate results, the pre-de–termined convergence criteria are 10^{-5} for each velocity and continuity equation and 10^{-7} for the energy equa–tion.

3.3.1 Mesh generation

Hexahedral mesh elements were chosen in this study due to their advantages over other types of mesh in terms of high solution stability and the lesser number of elements required to describe the domain [74]. Figure 10 depicts the meshed geometry of the entire thermal storage unit. As observed, fine mesh was generated close to tube walls to evaluate the hydrodynamic and thermal boundary layer and heat transfer rate into PCM. Compared to the fluid domain, the PCM domain has a

higher mesh density to capture free convection vortices and other flow characteristics induced during the charging process. Since the symmetric behavior, only a half part of the computational domain is meshed and simulated to save calculational time.

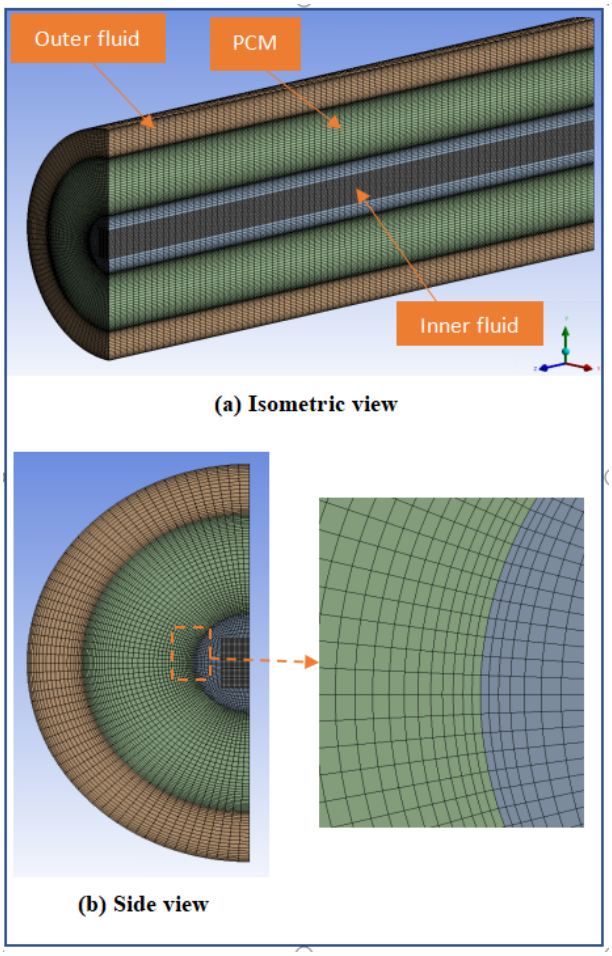

Figure 10. Grid generation for the current case study.

3.3.2 Mesh independent test

The mesh size independency test is performed on nano-PCM to acquire reliable numerical results. When the mesh density has an insignificant effect on numerical results, the mesh independence is approached. To test the mesh independency, four cases with element numbers 104160, 209440, 309120, and 399360 were adopted to simulate the charging process. These transient tests were numerically carried out using a time interval of 0.1 seconds. After choosing the sufficient grid size, time-step dependency was investigated using different time steps. Table 6 illustrates the comparison of melting periods for four different collections of space dis–cretization. It can be noticed that the discrepancy bet–ween the melting periods of cases 2 and 3 is 155 seconds; however, the discrepancy between cases 3 and 4 is 42 seconds, which is less than one-third the first difference. This implies that implementing an extra 90240 mesh elements to case 3 causes a change in melting time by only 0.44%. Therefore, considering computational time, a domain with a mesh element of 309120 is appropriate for numerical simulation.

Table 6: Mesh size selection.

Case	Number of elements	Number of nodes	Time step (s)	Melting time (s)	Relative error (%)
1	104160	110727	0.1	10451	9.56
2	209440	219186	0.1	9694	1.62
3	309120	321489	0.1	9539	-
4	399360	413991	0.1	9497	0.44

3.3.3 Time-independent test

In transient modeling, the time independence examination should be performed to ensure that the simulation outcomes are not dependent on the time. Time periods of 0.1 s, 0.01 s, and 0.001s are examined and compared to determine a suitable time period, see Table 7. The simulation outcomes show less than a 0.4% discrepancy when a time period of 0.001 seconds is applied. Therefore, a time period of 0.01 is chosen for the subsequent simulations to save computational cost.

Table 7: Time period independency carried out on a sample of hybrid nano-PCM.

Case	Number of elements	Number of nodes	Time step (s)	Melting time (s)	Relative error (%)
1	309120	321489	0.1	9539	0.8626
2	309120	321489	0.01	9622	-
3	309120	321489	0.001	9660	0.394

3.3.4 Verification

To verify the numerical simulation, the data of the melting process obtained from ANSYS Fluent was compared with the experimental data of the present work. HTF temperature was 62 °C and HTF flow rate was 3 kg/min, whereas the initial temperature of the hybrid nano-PCM (φ= 0.4%) was 30 °C. Figure 11 presents the comparison of the time-based average temperature of PCM, which was estimated using 20 thermocouples located in the midway (section B) of PCM storage, with that of the numerical data. The results show an acceptable agreement between them with an average deviation of 3%.

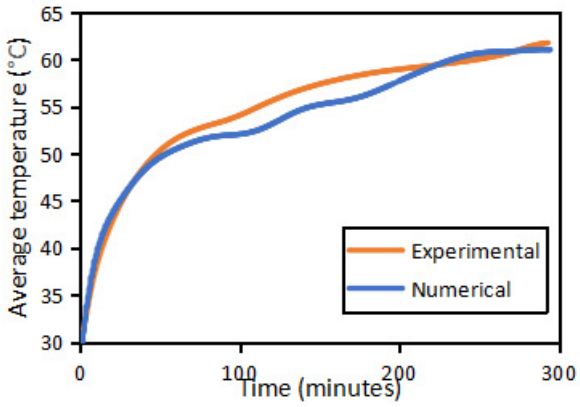

Figure 11. Comparison between experimental and numerical data.

4. RESULTS AND DISCUSSION

4.1 Mechanism of melting process

Figure 12 displays the temperature contours and streamline of the paraffin located at midway for HTF inlet temperature 70 °C and HTF mass flow 3 kg/min at t = 5 min, t = 30 min, t = 60 min, t = 90 min, t = 120 min, and t = 150 min. At the beginning of charging, the heat transfer between the annulus's hot surfaces and the two solid-liquid interfaces surrounding the solid region causes a temperature gradient. This gradient induces conduction heat transfer that during 5 min of charging, thin liquid layers adjacent to the inner and the intermediate tubes are created. By this time, conduction becomes the dominant heat transfer mode, and the solid phase occupies the most portion of the annulus. The upper part of PCM thermal storage has a higher average temperature than the lower part, which was between 42 °C and 39 °C. As time progresses, the average temperature difference between PCM's upper and lower parts increases. Afterward, at t = 30 min, the temperature of PCM at the top of the inner tube rises, which induces natural convection in this zone. This zone has two identical vertices in shape and size, rotating in opposite directions with one vortex on each side. Therefore, the molten zone expands upwardly in the annulus, and the vortices merge into the main larger ones. As can be seen from Figure 12, molten PCM surrounds the hot inner tube, and the hot intermediate tube moves upward and propagates into the solid PCM. The corresponding isotherms have distorted loop configurations located in the entire annulus as depicted at the 60 min. The circulation zone in the upper area of the inner tube merged with the convection zone in the upper zone of the intermediate tube. Once all the PCM in the upper half of the annulus melts, which occurs at t = 90 min, the remaining solid PCM in the lower half of the annulus starts to melt, and the liquid-solid interface moves away from the HTF tubes. After this stage, the melting rate reduces due to a reduction in buoyancy force. This can be noticed by reducing the average temperature difference between the top and bottom to 15 °C at t = 120 minutes; thus, the remaining PCM takes a longer time to melt. The melting process Proceeded until the PCM melted completely.

4.2 Effect of mass flow rate

The charging of the PCM for various mass flow rates was conducted at 70 °C HTF inlet temperature. Figures 13 and 12 depict the time-wise variation of average PCM temperature and liquid fraction at midway for mass flow rates of 3, 6, 9, and 12 kg/min. Generally, the average temperature increases with increased mass flow rate, ascribing to higher heat transfer coefficient in both tube and shell side attained at higher mass flow rates and thus higher heat flux into PCM. It can be noticed from Figure 14 that melting time decreases with increased mass flow rate. The time required for the total melting of the PCM is displayed in terms of mass flow rate in Table 8. One can notice that the total melting duration reduces up to 19% when the mass flow rate increases from 3 kg/min to 12 kg/min.

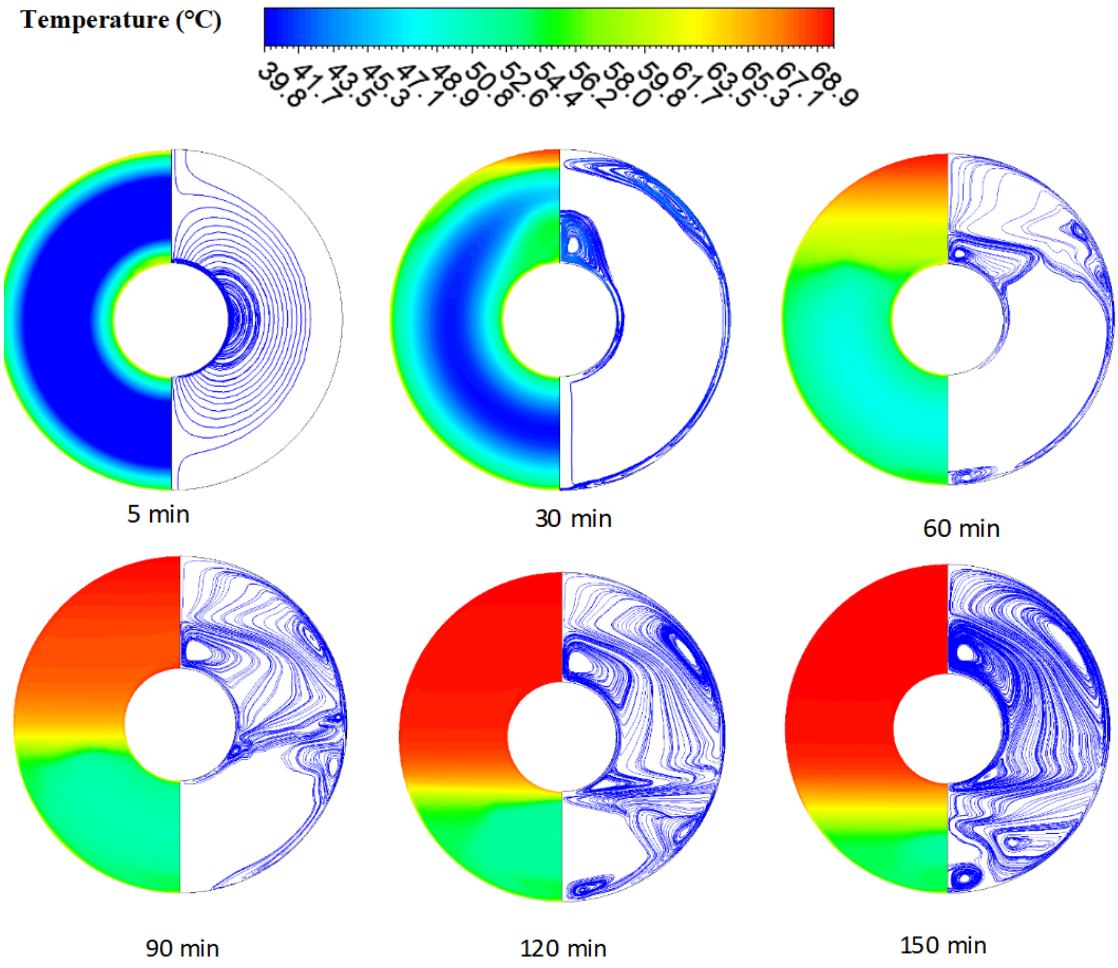

Figure 12. Temperature contour (left) and streamline (right) with time

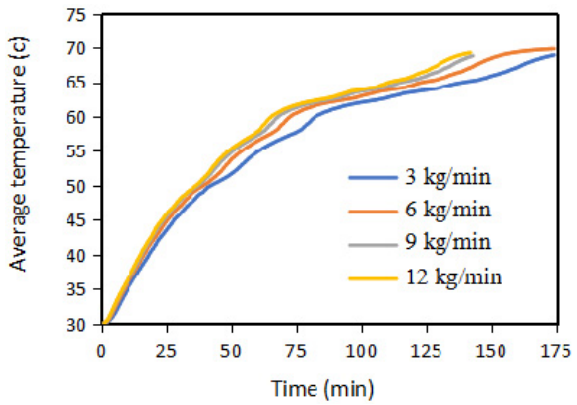

Figure 13. Average temperature vs time for different mass flow rates.

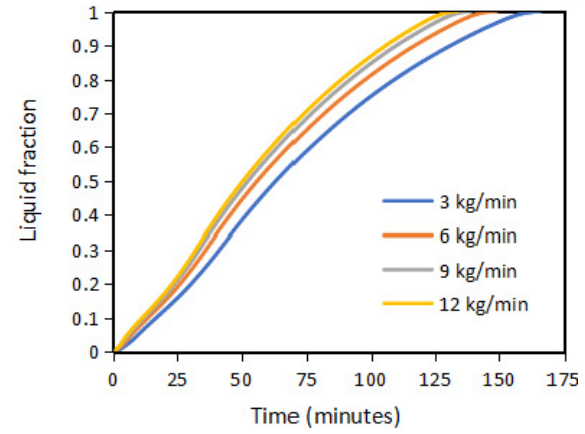

Figure 14. Liquid fraction over time for different mass flow rates.

Table 8. Effect of mass flow rate on total melting time at HTF temperature 70 °C.

Mass flow rate (kg/min)	Melting time (min)	Time reduction %
3	166	0
6	149	10.2
9	139	16.2
12	134	19.2

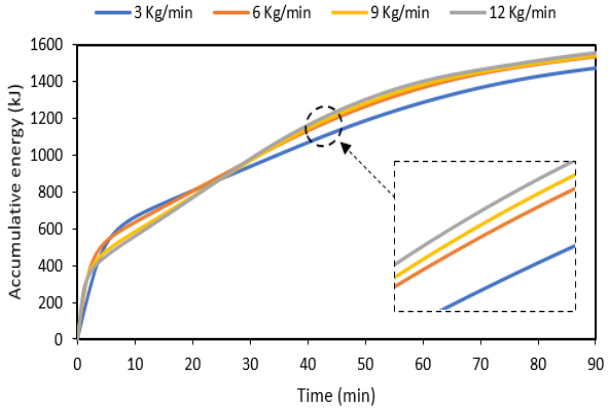

Figure 15. Heat recovery vs time for different mass flow rates.

Figure 15 depicts the cumulative energy retrieved during the charging process. As can be seen, there is a sharp increase of accumulative energy, latent and sensible, with time up to 10 min. This is due to the high-temperature difference between flow and PCM. Afterward, the inclination of the slop decreases, referring to a low heat rate. This was ascribed to an increase in the average temperature of PCM in the system from 30 °C to 40 °C. After 60 min of melting time, gradually less and less latent heat was charged, as shown by the smaller slope of the curve. It can also be noticed from the figure the stored energy increased with increased mass flow rate. A significant increase in heat recovery when mass flow rate increases from 3 kg/min to 6 kg/min. However, there is an insignificant increase in heat recovery when the mass flow rate increases above 6 kg/min. For 12 kg/min mass flow rate, the total quantity of heat energy retrieved was 1560 kJ, equivalent to 84.8% of maximum storage energy. This included solid, sensible heat retrieved from 30 °C to 53 °C, latent heat at 53 °C and sensible liquid heat from 53 °C to 78 °C. The maximum stored energy for charging the PCM from 30 °C to 78 °C was 1839 kJ.

To get more quantitative outcomes regarding the experiment, see Table 9. For different mass flow rates, this table includes total stored energy and the storage efficiency by which it can be predicted whether the heat exchanged is enough for thorough melting or not. Referring to Table 9, the storage efficiency increases with increased mass flow rate. The storage efficiency increases by 4.2% by increasing the mass flow rate from 3 to 12 kg/min.

Table 9. Effect of mass flow rate on the quantity of energy stored and efficiency at constant HTF inlet temperature 78 °C.

mass flow rate (kg/min)	Maximum heat storage (kJ)	Accumulative energy (kJ)	storage efficiency (%)
3	1839	1484	80.6
6	1839	1545.12	84
9	1839	1553.299	84.4
12	1839	1560.62	84.8

4.3 Effect of HTF inlet temperature

Various HTF inlet temperatures were employed to examine their effect on the PCM melting process. Figure 16 illustrates the time-wise variation of average PCM temperature for HTF inlet temperatures of 62 °C, 70 °C, and 78 °C at mass flow rates of 3 kg/min and 12 kg/min. Apparently, the average temperature of PCM increases with increased HTF temperature. This is because increasing HTF temperature increases the tem–perature difference between HTF and PCM, which is considered the driving force of the heat transfer rate.

At a mass flow rate of 3 kg/min, the Elapsed time to approach 60 °C in a system is 264, 83, and 54 minutes, respectively, for HTF inlet temperatures of 62 °C, 70 °C, 78 °C. It can also be noticed from Figure 14 that the changing HTF inlet temperature at a high mass flow rate has more effect on the PCM average temperature than at a low mass flow rate.

Moreover, Figure 17 shows that charging time dec–reases with increased HTF temperature. Quanti–tatively, the total melting time can be decreased up to 60 % for HTF inlet temperature 78 °C, see Table 10. This indi–cates that increasing HTF inlet temperature has more effect on melting rate than increasing mass flow rate.

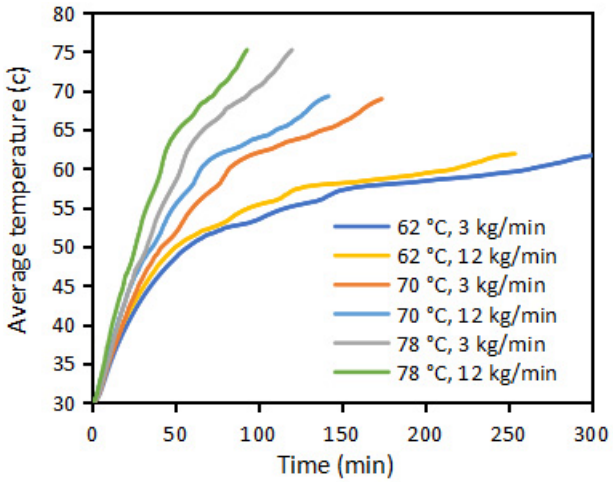

Figure 16. The average temperature over time for different inlet temperatures and mass flow rates.

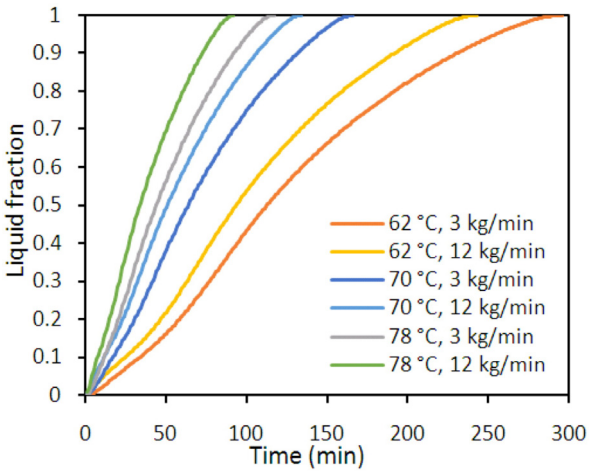

Figure 17. Liquid fraction vs time for different HTF inlet temperatures and mass flow rate.

Table 10. Effect of HTF temperature on total melting time at 3 kg/min mass flow rate.

Temperature of HTF (°C)	Time (min)	Time reduction %
62	296	0
70	166	43.9
78	117	60.4

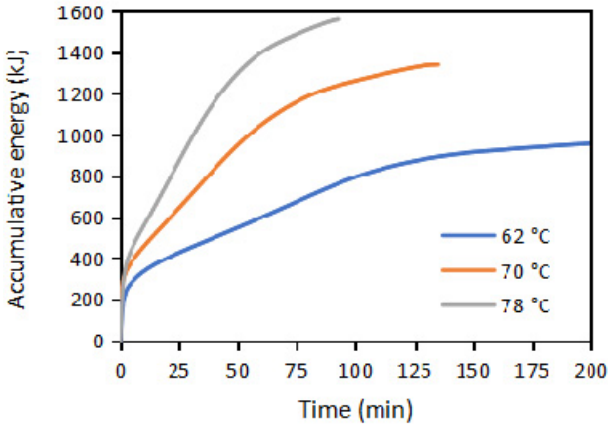

Figure 18. Heat recovery over time for different inlet temperatures.

Figure 18 shows the accumulated energy acquired from hot water during the charging process. As expected, the higher the HTF temperature, the higher the quantity of cumulative energy that can be gained. The results listed in Table 11 indicate that the theoretical efficiency increases as the inlet temperature rises. For instance, theoretical efficiencies are 61.7%, 78.3%, and 84.8% for inlet temperatures of 62 °C, 70 °C and 78 °C, respectively. By definition, when the storage efficiency reaches one, the energy needed to melt the entire PCM is supplied. Thus, the higher the storage efficiency, the larger the quantity of PCM will melt.

Table 11. Comparison of storage efficiency for different HTF inlet temperatures.

HTFT (°C)	Maximum heat storage (kJ)	Accumulative energy (kJ)	Storage efficiency (%)
62	1581.6	975.915	61.7
70	1710.4	1340.7	78.3
78	1839	1560.62	84.8

4.4 The effect of adding hybrid nanoparticles

The outcomes are shown in terms of time-dependent average PCM temperature, temperature contour, liquid fraction contour, and profile of liquid fraction for five various volume fractions values of hybrid nanoparticle (i.e., φ = 0 %, 0.4 %, 0.8 %, 1.6%, and 3.2%) and at HTF inlet temperature 70 °C and mass flow rate 3 kg/min. Figures 19–22 demonstrate the influence of adding alumina/CuO hybrid nanoparticles on average PCM temperature, isotherms, liquid-fraction contours, and liquid fraction curves over various melting durations. The result showed that increasing the volume fraction of hybrid nanoparticles enhances the rate of heat transfer and thus reduces the period for complete melting. This is because dispersing nanoparticles boosts the thermal conductivity and viscosity of the mixture.

The increase in viscosity leads to an increase in the shear stress between layers of the mixture, which resists liquid movement and reduces the temperature gradient. Therefore, if the rise in thermal conductivity is higher than the reduction in temperature gradient, a larger quan–tity of heat is absorbed by nano-PCM. However, it is observed that dispersing hybrid nanoparticles minimizes the conduction dominancy and enhances convection current, causing the isotherms to appear more deformed.

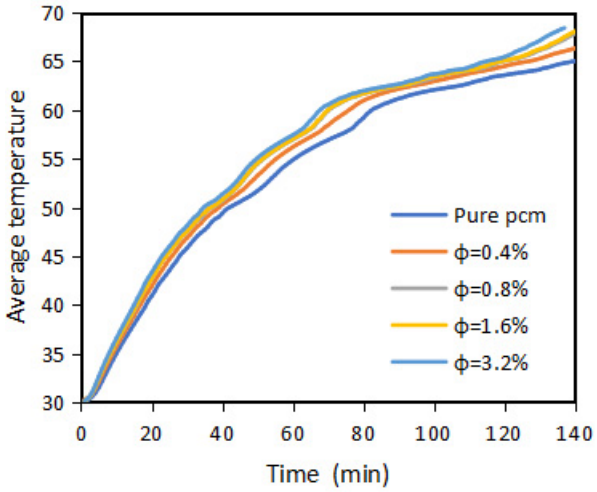

Figure 19. Average temperature vs. time for different nano concentrations.

This can be observed from the isotherms of hybrid nano-PCM (φ = 0.4, 0.8, 1.6, 3.2%) compared to pure PCM during all time duration in Figure 20. Regarding liquid-solid interface shape, there is an insignificant difference between hybrid nano-PCM and pure PCM throughout the early time of melting (e.g., t = 15 min), where heat transfer is mostly by conduction, as illustrated in Figure 21. However, the differences are more noticeable after 30 minutes of melting due to convection domination. Generally, the change in isotherms and liquid-fraction because of dispersing hybrid nanoparticles are more appreciable as time passes and/or rises in volume fraction.

The liquid fraction, which shows the amount of molten PCM, is crucial in evaluating the performance of thermal storage unit-based PCM. Figure 22 illustrates the time-wise variation of the liquid fraction during the melting phase using PCM and hybrid nano-PCM for HTFT = 70 °C and mass flow = 3 kg/min. The figure implies that implementing Al_2O_3/CuO hybrid nanoparticles of concentration (φ = 0.4%, 0.8%, 1.6%, and 3.2%) does not display a considerable difference at the early melting period. However, as time progresses, a higher liquid fraction is noticed compared to pure PCM. Table 12 lists the total time reduction percentages in hybrid nano-PCM relative to the corresponding values in pure PCM. Pure PCM takes 166 min to melt for HTFT = 70 °C completely. Hybrid nano-PCM with φ = 0.4%, 0.8%, 1.6%, and 3.6% takes less time and produces a total period reduction ranging from 10% to 19% compared to those of pure PCM. Therefore, the existence of hybrid nanoparticles considerably contributes to approaching the complete melting state within a shorter duration.

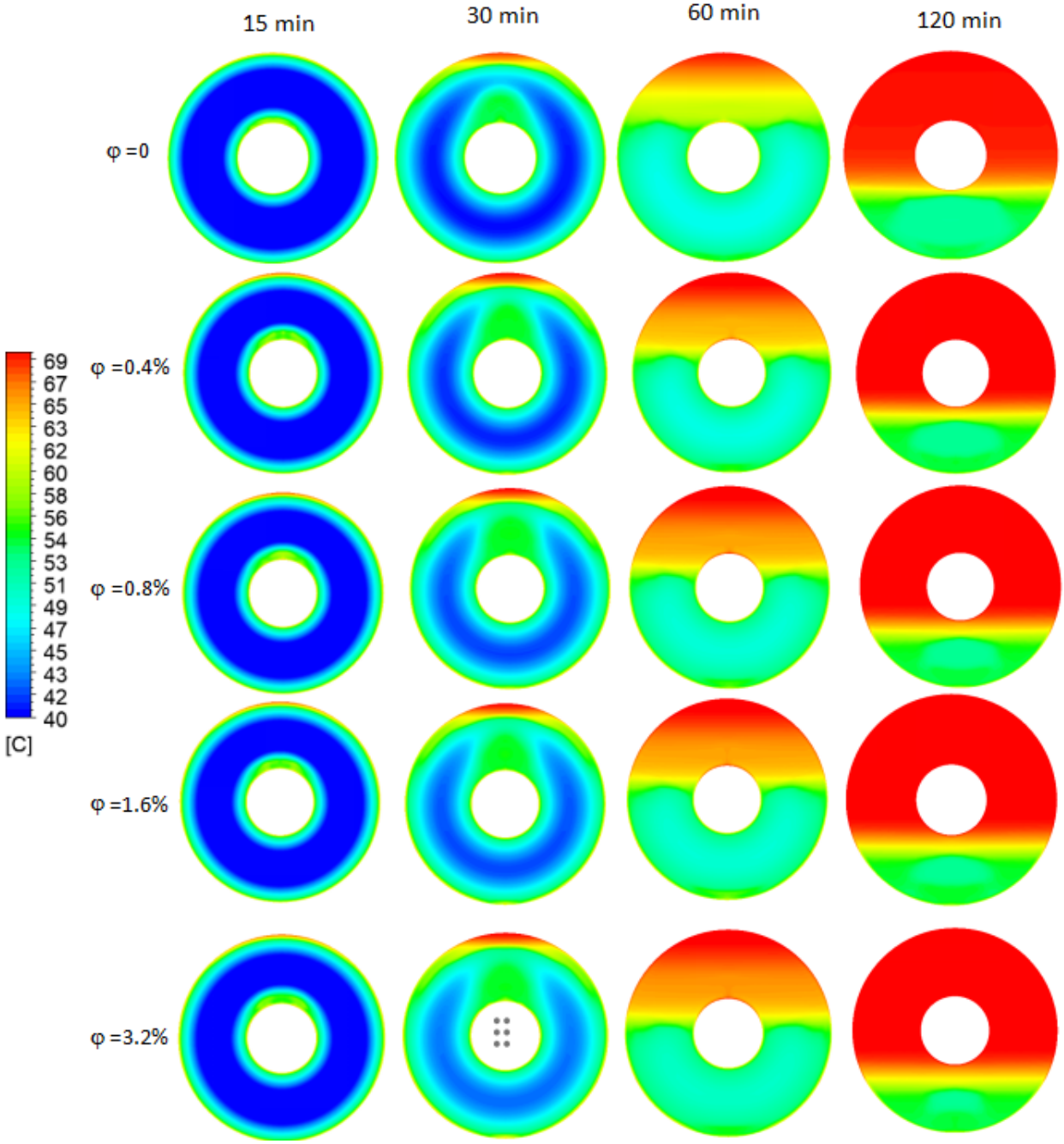

Figure 20. Temperature contour over time for various volume fraction of hybrid nanoparticle at 70 °C HTF and 3 kg/min mass flow rate.

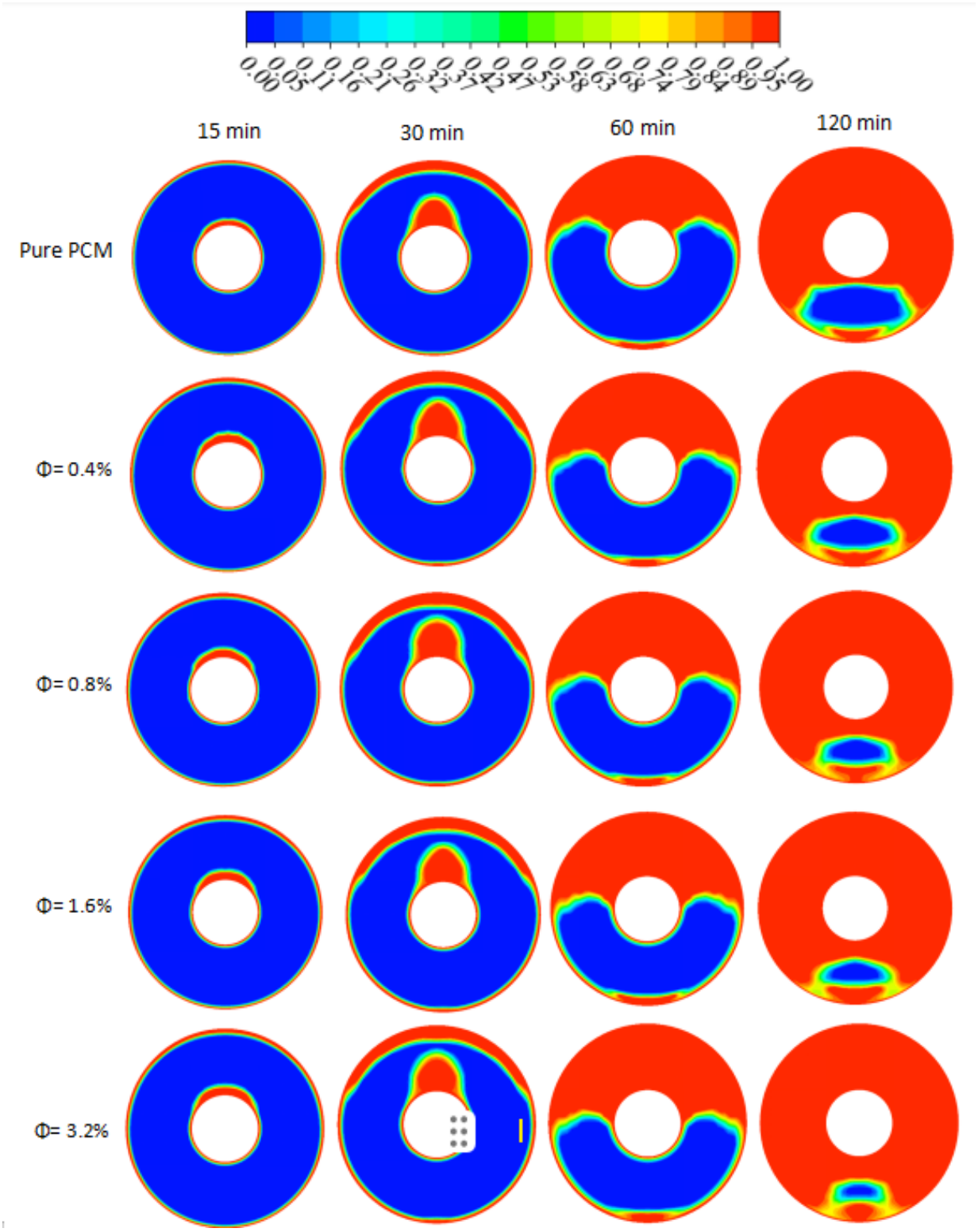

Figure 21. Liquid fraction at different time duration and different volume fractions of hybrid nanoparticles throughout melting of the mixture at 70 °C HTF and 3 kg/min mass flow rate.

It is important to mention that using nanoparticles to decrease melting time has several contributions to the design and performance of storage systems. Firstly, a shorter melting time enables faster charging of the sto–rage unit, thereby enhancing its efficiency. Secondly, this facilitates the storage system's ability to respond quickly to fluctuations in thermal energy demand or supply, making it advantageous for integration with re–newable energy sources and enhancing load manage–ment. Lastly, the reduced melting time allows for the design of storage devices with smaller volumes or lower amounts of PCM, thereby minimizing system cost.

Table 12. Effect of hybrid nanoparticles concentration on total melting time at HTF 70 °C.

Concentration %	Time (min)	Time reduction %
0	166	0
0.4	149	10.2
0.8	143	13.8
1.6	141	15
3.2	135	18.6

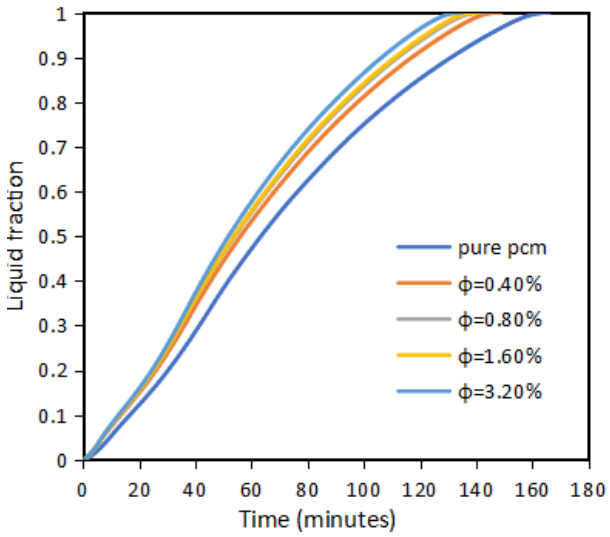

Figure 22. liquid fraction variation over time for various volume fractions at 70°C HTFT.

5. CONCLUSION

According to the findings of the current numerical and experimental study of the melting of hybrid nano PCM inside triplex tube heat storage. The upcoming conclusions are obtained:

- Heat transfer and, thus, melting time are directly dependent on the HTF inlet temperature. The current investigation demonstrates that the total melting time can be decreased by up to 60% by boosting the inlet HTF temperature from 62 °C to 78 °C.
- The total charging time was reduced by 19 % as the mass flow rate increased from 3 kg/min to 12 kg/min.
- Stored energy in PCM increased with increased mass flow rate and/or increased HTF inlet temperature.
- 10.2%, 13.8%, 15%, and 18.6% reduction in melting duration were obtained for PCM with the hybrid nanoparticle of volume fraction of 0.4%, 0.8%, 1.6%, and 3.2%, respectively.
- Because of conduction dominancy at the early stages of melting, the interfaces between liquid and solid are similar in shape and size for all volume fractions. As time progresses, free convection domination influences the configuration of the phase front and cause to accelerate charging of the solid PCM.

Data availability

Data will be provided upon request through e-mail to Ibrahim E. Sadiq (**me.19.27@grad.uotechnology.edu.iq**)

Conflicts of interest

The authors state they have no conflicts of Interest.

Funding statement

There was no particular grant for this work from any funding organization in the public, private, or nonprofit sectors.

REFERENCES

[1] S. Bezari, S. Bekkouche, A. Benchatti, Investigation and improvement for a solar greenhouse using sensible heat storage material, FME Transactions, 49(1) (2021) 154-162.

[2] S. Kumar, R. B. Anand, A case study on damage detection of wind turbine composite blade, FME Transactions, 47(1) (2019) 135-141.

[3] A. Khudhair, F. Hatem, D. Mohammed Ridha, Enhancement of Thermal Storage Properties of Phase Change Material by Using Metallic Swarf, Engineering and Technology Journal, 36(5A) (2018) 586-595.

[4] Akram H. Abed, Thermal storage efficiency enhancement for solar air heater using a combined SHSm and PCM cylindrical capsules system: experimental investigation, Engineering and Technology Journal, 34(5 Part (A) Engineering) (2016).

[5] M. Tawalbeh, H. A. Khan, A. Al-Othman, F. Almomani, S. Ajith, A comprehensive review on the recent advances in materials for thermal energy storage applications, International Journal of Thermofluids, (2023) 100326.

[6] M. M. Farid, A. M. Khudhair, S. A. K. Razack, S. Al-Hallaj, A review on phase change energy storage: materials and applications, Energy conversion and management, 45(9-10) (2004) 1597-1615.

[7] A. N. Sadr, M. Shekaramiz, M. Zarinfar, A. Esmaily, H. Khoshtarash, D. Toghraie, Simulation of mixed-convection of water and nano-encapsulated phase change material inside a square cavity with a rotating hot cylinder, Journal of Energy Storage, 47 (2022) 103606.

[8] Sattar ALJABAIR, Israa ALESBE and Sahira Hasan IBRAHIM, Review on latent thermal energy storage using phase change material, Journal of Thermal Engineering, 9(1) (2021) 247-256.

[9] M. Sun, T. Liu, H. Sha, M. Li, T. Liu, X. Wang, G. Chen, J. Wang, D. Jiang, A review on thermal energy storage with eutectic phase change materials: Fundamentals and applications, Journal of Energy Storage, 68 (2023) 107713.

[10] M. Samykano, Role of phase change materials in thermal energy storage: Potential, recent progress and technical challenges, Sustainable Energy Technologies and Assessments, 52 (2022) 102234.

[11] G. Alva, L. Liu, X. Huang, G. Fang, Thermal energy storage materials and systems for solar energy applications, Renewable and Sustainable Energy Reviews, 68 (2017) 693-706.

[12] [M. G. Gado, H. Hassan, Energy-saving potential of compression heat pump using thermal energy storage of phase change materials for cooling and heating applications, energy, 263 (2023) 126046.

[13] Y. Liu, R. Zheng, J. Li, High latent heat phase change materials (PCMs) with low melting temperature for thermal management and storage of electronic

devices and power batteries: Critical review, Renewable and Sustainable Energy Reviews, 168 (2022) 112783.

[14] A. Abhat, Low temperature latent heat thermal energy storage: heat storage materials, Solar energy, 30(4) (1983) 313-332.

[15] A. M. Abdulateef, S. Mat, J. Abdulateef, K. Sopian, A. A. Al-Abidi, Geometric and design parameters of fins employed for enhancing thermal energy storage systems: a review, Renewable and Sustainable Energy Reviews, 82 (2018) 1620-1635.

[16] G. S. Sodhi, P. Muthukumar, Compound charging and discharging enhancement in multi-PCM system using nonuniform fin distribution, Renewable Energy, 171 (2021) 299-314.

[17] X. Luo, J. Gu, H. Ma, Y. Xie, A. Li, J. Wang, R. Ding, Numerical study on enhanced melting heat transfer of PCM by the combined fractal fins, Journal of Energy Storage, 45 (2022) 103780.

[18] S. Zhang, L. Pu, S. Mancin, M. Dai, L. Xu, Role of partial and gradient filling strategies of copper foam on latent thermal energy storage: An experimental study, energy, 255 (2022) 124517.

[19] Z. Haddad, F. Iachachene, M. A. Sheremet, E. Abu-Nada, Numerical investigation and optimization of melting performance for thermal energy storage system partially filled with metal foam layer: New design configurations, Applied Thermal Engineering, 223 (2023) 119809.

[20] H. Behi, M. Behi, A. Ghanbarpour, D. Karimi, A. Azad, M. Ghanbarpour, M. Behnia, Enhancement of the thermal energy storage using heat-pipe-assisted phase change material, Energies, 14(19) (2021) 6176.

[21] P. Peng, Y. Wang, F. Jiang, Numerical study of PCM thermal behavior of a novel PCM-heat pipe combined system for Li-ion battery thermal management, Applied Thermal Engineering, 209 (2022) 118293.

[22] N. H. Abu-Hamdeh, A. Shafee, A. A. Azhari, A. H. Milyani, A. M. Hussin, Modification of storage system to reach faster solidification with impose of nanoparticles, Journal of Energy Storage, 62 (2023) 106823.

[23] R. Qahiti, A. Almarashi, W. Hamali, Thermal behavior of nanoparticle enhanced phase change material discharging in existence of complex geometry, Journal of Energy Storage, 59 (2023) 106450.

[24] A. H. Mosaffa, F. Talati, H. Basirat Tabrizi, M. A. Rosen, Analytical modeling of PCM solidification in a shell and tube finned thermal storage for air conditioning systems, Energy and Buildings, 49 (2012) 356-361.

[25] M. K. Rathod, J. Banerjee, Thermal performance enhancement of shell and tube Latent Heat Storage Unit using longitudinal fins, Applied Thermal Engineering, 75 (2015) 1084-1092.

[26] A. A. Rabienataj Darzi, M. Jourabian, M. Farhadi, Melting and solidification of PCM enhanced by radial conductive fins and nanoparticles in cylindrical annulus, Energy Conversion and Management, 118 (2016) 253-263.

[27] S. Lohrasbi, M. Gorji-Bandpy, D. D. Ganji, Thermal penetration depth enhancement in latent heat thermal energy storage system in the presence of heat pipe based on both charging and discharging processes, Energy Conversion and Management, 148 (2017) 646-667.

[28] V. Safari, H. Abolghasemi, L. Darvishvand, B. Kamkari, Thermal performance investigation of concentric and eccentric shell and tube heat exchangers with different fin configurations containing phase change material, Journal of Energy Storage, 37 (2021).

[29] V. Safari, H. Abolghasemi, B. Kamkari, Experimental and numerical investigations of thermal performance enhancement in a latent heat storage heat exchanger using bifurcated and straight fins, Renewable Energy, 174 (2021) 102-121.

[30] Z. Wang, Z. Zhang, L. Jia, L. Yang, Paraffin and paraffin/aluminum foam composite phase change material heat storage experimental study based on thermal management of Li-ion battery, Applied Thermal Engineering, 78 (2015) 428-436.

[31] W. Q. Li, Z. G. Qu, Y. L. He, W. Q. Tao, Experimental and numerical studies on melting phase change heat transfer in open-cell metallic foams filled with paraffin, Applied Thermal Engineering, 37 (2012) 1-9.

[32] Noor Hamza, Sattar Aljabair, Review of Heat transfer enhancement using hybrid Nano fluid or twisted tape insert, Journal of Mechanical Engineering Research and Developments, 44, No. 5 (2021) 345-357.

[33] S. Saha, S. Bansal, M. Khanuja, Classification of nanomaterials and their physical and chemical nature, in: Nano-enabled Agrochemicals in Agriculture, Elsevier, 2022, pp. 7-34.

[34] J. M. Khodadadi, S. F. Hosseinizadeh, Nanoparticle-enhanced phase change materials (NEPCM) with great potential for improved thermal energy storage, International Communications in Heat and Mass Transfer, 34(5) (2007) 534-543.

[35] S. Y. Wu, H. Wang, S. Xiao, D. S. Zhu, An investigation of melting/freezing characteristics of nanoparticle-enhanced phase change materials, Journal of Thermal Analysis and Calorimetry, 110(3) (2011) 1127-1131.

[36] R. J. Warzoha, A. S. Fleischer, Improved heat recovery from paraffin-based phase change materials due to the presence of percolating graphene networks, International Journal of Heat and Mass Transfer, 79 (2014) 314-323.

[37] Noor Hamza, Sattar Aljabair, Numerical and Experimental Investigation of Heat Transfer Enhancement by Hybrid Nanofluid and Twisted Tape, Engineering and Technology Journal, 41(1) (2022) 69-85.

[38] M. Alizadeh, K. Hosseinzadeh, H. Mehrzadi, D. D. Ganji, Investigation of LHTESS filled by Hybrid

nano-enhanced PCM with Koch snowflake fractal cross section in the presence of thermal radiation, Journal of Molecular Liquids, 273 (2019) 414-424.

[39] K. Hosseinzadeh, M. Alizadeh, M. H. Tavakoli, D. D. Ganji, Investigation of phase change material solidification process in a LHTESS in the presence of fins with variable thickness and hybrid nanoparticles, Applied Thermal Engineering, 152 (2019) 706-717.

[40] Z. Khan, Z. Ahmad Khan, Experimental and numerical investigations of nano-additives enhanced paraffin in a shell-and-tube heat exchanger: A comparative study, Applied Thermal Engineering, 143 (2018) 777-790.

[41] M. A. Said, H. Hassan, Effect of using nanoparticles on the performance of thermal energy storage of phase change material coupled with air-conditioning unit, Energy Conversion and Management, 171 (2018) 903-916.

[42] P. Kumar, R. Elakkiyadasan, N. Sathishkumar, G. Prabhu, T. Balasubramanian, Performance enhancement of a domestic refrigerator with Nanoparticle Enhanced PCM over the condenser side, FME Transactions, 48(3) (2020) 620-627.

[43] A. J. Abdulhamed, N. M. Adam, M. Z. A. Ab-Kadir, A. A. Hairuddin, Review of solar parabolic-trough collector geometrical and thermal analyses, performance, and applications, Renewable and Sustainable Energy Reviews, 91 (2018) 822-831.

[44] [44] A. Fudholi, K. Sopian, A review of solar air flat plate collector for drying application, Rene–wable and Sustainable Energy Reviews, 102 (2019) 333-345.

[45] X. Cao, N. Zhang, Y. Yuan, X. Luo, Thermal performance of triplex-tube latent heat storage exchanger: simultaneous heat storage and hot water supply via condensation heat recovery, Renewable Energy, 157 (2020) 616-625.

[46] T. Nascimento Porto, J. M. Delgado, A. S. Guimarães, H. L. Fernandes Magalhães, G. Moreira, B. Brito Correia, T. Freire de Andrade, A. G. Barbosa de Lima, Phase change material melting process in a thermal energy storage system for applications in buildings, Energies, 13(12) (2020) 3254.

[47] A. A. Al-Abidi, S. Mat, K. Sopian, M. Sulaiman, A. T. Mohammad, Experimental study of PCM melting in triplex tube thermal energy storage for liquid desiccant air conditioning system, energy and buildings, 60 (2013) 270-279.

[48] N. H. Mohamed, F. S. Soliman, H. El Maghraby, Y. M. Moustfa, Thermal conductivity enhancement of treated petroleum waxes, as phase change material, by α nano alumina: Energy storage, Renewable and Sustainable Energy Reviews, 70 (2017) 1052-1058.

[49] P. M. Kumar, K. Mylsamy, K. Prakash, M. Nithish, R. Anandkumar, Investigating thermal properties of Nanoparticle Dispersed Paraffin (NDP) as phase change material for thermal energy storage, Materials Today: Proceedings, 45 (2021) 745-750.

[50] E. Bellos, C. Tzivanidis, Thermal analysis of parabolic trough collector operating with mono and hybrid nanofluids, Sustainable Energy Technologies and Assessments, 26 (2018) 105-115.

[51] K. Khanafer, K. Vafai, A critical synthesis of thermophysical characteristics of nanofluids, International journal of heat and mass transfer, 54(19-20) (2011) 4410-4428.

[52] G. Batchelor, The effect of Brownian motion on the bulk stress in a suspension of spherical particles, Journal of fluid mechanics, 83(1) (1977) 97-117.

[53] M. Amani, P. Amani, A. Kasaeian, O. Mahian, S. Wongwises, Thermal conductivity measurement of spinel-type ferrite MnFe2O4 nanofluids in the presence of a uniform magnetic field, Journal of Molecular Liquids, 230 (2017) 121-128.

[54] A. O. Elsayed, Numerical study on performance enhancement of solid–solid phase change materials by using multi-nanoparticles mixtures, Journal of Energy Storage, 4 (2015) 106-112.

[55] A. V. Arasu, A. S. Mujumdar, Numerical study on melting of paraffin wax with Al2O3 in a square enclosure, International Communications in Heat and Mass Transfer, 39(1) (2012) 8-16.

[56] O. A. Alawi, N. A. C. Sidik, H. W. Xian, T. H. Kean, S. N. Kazi, Thermal conductivity and viscosity models of metallic oxides nanofluids, International Journal of Heat and Mass Transfer, 116 (2018) 1314-1325.

[57] R. S. Vajjha, D. K. Das, Experimental determination of thermal conductivity of three nanofluids and development of new correlations, International Journal of Heat and Mass Transfer, 52(21-22) (2009) 4675-4682.

[58] Israa Y. Daood, Effects of Nano-Fluids Types, Volume Fraction of Nanoparticles, and Aspect Ratios on Natural Convection Heat Transfer in Right-Angle Triangular Enclosure, Eng. And Tech. Journal, 28(16) (2010) 5365-5388.

[59] A. Babapoor, G. Karimi, Thermal properties measurement and heat storage analysis of paraffin nanoparticles composites phase change material: Comparison and optimization, Applied Thermal Engineering, 90 (2015) 945-951.

[60] A. Babapoor, G. Karimi, S. Sabbaghi, Thermal characteristic of nanocomposite phase change materials during solidification process, Journal of Energy Storage, 7 (2016) 74-81.

[61] F. Agyenim, P. Eames, M. Smyth, Experimental study on the melting and solidification behaviour of a medium temperature phase change storage material (Erythritol) system augmented with fins to power a LiBr/H2O absorption cooling system, Renewable Energy, 36(1) (2011) 108-117.

[62] M. J. Hosseini, M. Rahimi, R. Bahrampoury, Experimental and computational evolution of a shell and tube heat exchanger as a PCM thermal storage system, International Communications in Heat and Mass Transfer, 50 (2014) 128-136.

[63] R. J. Moffat, Describing the uncertainties in experimental results, Experimental thermal and fluid science, 1(1) (1988) 3-17.

[64] A. Brent, V. R. Voller, K. Reid, Enthalpy-porosity technique for modeling convection-diffusion phase change: application to the melting of a pure metal, Numerical Heat Transfer, Part A Applications, 13(3) (1988) 297-318.

[65] Z.-X. Gong, S. Devahastin, A. S. Mujumdar, Enhanced heat transfer in free convection-dominated melting in a rectangular cavity with an isothermal vertical wall, Applied Thermal Engineering, 19(12) (1999) 1237-1251.

[66] S. Seddegh, X. Wang, A. D. Henderson, A comparative study of thermal behaviour of a horizontal and vertical shell-and-tube energy storage using phase change materials, Applied Thermal Engineering, 93 (2016) 348-358.

[67] F. Afsharpanah, M. Izadi, F. A. Hamedani, S. S. Mousavi Ajarostaghi, W. Yaïci, Solidification of nano-enhanced PCM-porous composites in a cylindrical cold thermal energy storage enclosure, Case Studies in Thermal Engineering, 39 (2022).

[68] M. Sheikholeslami, Numerical analysis of solar energy storage within a double pipe utilizing nanoparticles for expedition of melting, Solar Energy Materials and Solar Cells, 245 (2022) 111856.

[69] Z. Li, A. Shahsavar, A. A. A. A. Al-Rashed, P. Talebizadehsardari, Effect of porous medium and nanoparticles presences in a counter-current triple-tube composite porous/nano-PCM system, Applied Thermal Engineering, 167 (2020).

[70] A. Mourad, A. Aissa, A. M. Abed, G. F. Smaisim, D. Toghraie, M. A. Fazilati, O. Younis, K. Guedri, A. a. Alizadeh, The numerical analysis of the melting process in a modified shell-and-tube phase change material heat storage system, Journal of Energy Storage, 55 (2022) 105827.

[71] S. Patankar, Numerical heat transfer and fluid flow, Washington, DC: Hemisphere, 1980, Google Scholar| Crossref.

[72] A. A. Al-Abidi, S. B. Mat, K. Sopian, M. Sulaiman, A. T. Mohammed, CFD applications for latent heat thermal energy storage: a review, Renewable and sustainable energy reviews, 20 (2013) 353-363.

[73] M. Rahimi, A. Ranjbar, M. Hosseini, M. Abdollahzadeh, Natural convection of nanoparticle–water mixture near its density inversion in a rectangular enclosure, International Communications in Heat and Mass Transfer, 39(1) (2012) 131-137.

[74] J. F. Shepherd, C. R. Johnson, Hexahedral mesh generation constraints, Engineering with Computers, 24(3) (2008) 195-213.

NOMENCLATURE

Abbreviation

PCM	Phase change material
TTHS	Triplex tube heat storage
HTF	Heat transfer fluid
HTFT	Heat transfer fluid temperature
DSC	Differential scanning calorimetry

Symbols

T	Temperature (°C)
P	Pressure (pa)
$\vec{V}$	Fluid velocity (m/sec)
$\vec{S}$	Damping term of Darcy's law
$\vec{g}$	Gravity (m/sec2)
t	time
C_p	Specific heat (J/kg °C)
k	Thermal conductivity (w/m °C)
h	sensible enthalpy
L	Latent heat of fusion (J/kg)
H	Enthalpy of material (J /kg)
ΔH	Latent heat content

Greek symbols

φ	Volume fraction
β	Thermal expansion factor (1/K)
ρ	density (kg/m3)
μ	Fluid viscosity (pa.s)
λ	Liquid fraction

Subscripts

hnp	Hybrid nanoparticles
np1	Aluminum oxide nanoparticles
np2	Copper oxide nanoparticles
ref	Reference value
npcm	Nano-phase change material
hnpcm	Hybrid nano phase change material

УТИЦАЈ ДИСПЕРЗИЈЕ ХИБРИДНИХ НАНОЧЕСТИЦА Al_2O_3/CuO НА ПРОЦЕС ТОПЉЕЊА ПЦМ-А У ТРИПЛЕКС ЦЕВИ ЗА СКЛАДИШТЕЊЕ ТОПЛОТЕ

И.Е. Садик, С. Алцабаји, А.А. Карамалах

Овим истраживањем спроведено је експериментално и теоријско испитивање карактеристика топљења материјала са променом фазе у троструком цевном акумулацији топлоте. Тродимензионални модел је нумерички симулиран коришћењем софтвера Ансис Флуент. За решавање фазног прелаза парафинског воска изабрана је метода енталпијске порозности. Мешавина CuO и Al_2O_3 хибридних наноадитива једнаке запремине је коришћена као проводни материјал за побољшање преноса топлоте у ПЦМ, што се може сматрати оригиналношћу ове студије. Најпре је извршена анализа диференцијалног скенирајућег калориметра (ДСЦ) да би се одредила термофизичка својства парафина. У парафину су дисперговане различите запреминске концентрације од 0,4%, 0,8%, 1,6% и 3,2%. Поред тога, експери–мент је изведен под различитим масеним протоком и температурама улазног флуида да би се испитао утицај ова два параметра на брзину фазног прелаза. Резултати показују да додавање Al_2O_3/CuO хиб–

ридне наночестице запреминског удела од 0,4-3,2% узрокује смањење укупног времена пуњења између 10% и 19%. Резултат је такође показао да се термијска ефикасност повећава са 61,7% на 84,8% како се улазна температура флуида за пренос топлоте (ХТФ) повећава са 62°C на 78°C.